

GMRT observations of *X*-shaped radio sources

Dharam Vir Lal^{*} and A. Pramesh Rao

National Centre for Radio Astrophysics (NCRA-TIFR), Pune University campus, Ganeshkhind, Pune - 411 007, India.

Accepted 1988 December 15. Received 1988 December 14; in original form 1988 October 11

ABSTRACT

We present results from a study of *X*-shaped sources based on observations using the Giant Metrewave Radio Telescope (GMRT). These observations were motivated by our low frequency study of 3C 223.1 (Lal & Rao 2005), an *X*-shaped radio source, which showed that the wings (or low-surface-brightness jets) have flatter spectral indices than the active lobes (or high-surface-brightness jets), a result not easily explained by most models. We have now obtained GMRT data at 240 and 610 MHz for almost all the known *X*-shaped radio sources and have studied the distribution of the spectral index across the sources. While the radio morphologies of all the sources at 240 and 610 MHz show the characteristic *X*-shape, the spectral characteristics of the *X*-shaped radio sources, seem to fall into three categories, namely, sources in which (A) the wings have flatter spectral indices than the active lobes, (B) the wings and the active lobes have comparable spectral indices, and (C) the wings have steeper spectral indices than the active lobes. We discuss the implications of the new observational results on the various formation models that have been proposed for *X*-shaped sources.

Key words: galaxies: active – galaxies: formation – radio continuum: galaxies

1 INTRODUCTION

A peculiar and a very small subclass of extragalactic radio sources called as the *X*-shaped or ‘winged’ sources are characterised by two low-surface-brightness lobes (the ‘wings’) oriented at an angle to the ‘active’, or high-surface-brightness radio lobes, giving the total source an ‘*X*’ shape. These two sets of lobes usually pass symmetrically through the centre of the associated host galaxy. Merritt & Ekers (2002) noted that majority of these sources are of FR II (Fanaroff & Riley 1974) and rest are either FR I or mixed.

X-shaped sources seem to reside in different types of host galaxies. Nearly half of these sources reside in fairly elliptical host galaxies. The hosts of some of these were reported to be slightly elongated and in several prominent dust disks have been found (Rottmann 2001). The environments of *X*-shaped sources seem to be poor. Almost all the sources are no part of rich clusters of groups. Rottmann (2001) reported, five (NGC 326, 3C 223.1, 4C 48.29, B1059+169 3C 315 and 3C 403) of these sources to be located in galaxy groups or clusters. However the density of these galaxy groups or clusters is low in all cases. The X-ray result shows that only one (NGC 326) is embedded in hot cluster gas, and this is the only source having a close companion galaxy.

Radio observations of these *X*-shaped sources show a high degree of polarisation (15%–30%) in the wings

and an apparent magnetic field structure parallel to the edge of the source and along the length of the wings (Dennett-Thorpe et al. 2002). Further high frequency and high resolution radio polarisation images showed field lines wrapping around the edges, as well as complex internal structure (3C 223.1: Black et al. 1992; 3C 315: Högbom 1979; etc.).

Several authors have attempted to explain the unusual structure in *X*-shaped sources. The first attempt was made by Rees (1978), who suggested that the jet direction precesses due to a realignment caused by the accretion of gas with respect to the central black hole axis. Dennett-Thorpe et al. (2002) discussed four possible scenarios for the formation of such radio morphology: (1) backflow from the active lobes into the wings (Leahy & Williams 1984; Capetti et al. 2002); (2) slow conical precession of the jet axis (Parma, Ekers & Fanti 1985; Mack et al. 1994); (3) reorientation of the jet axis during which flow continues; and (4) reorientation of the jet axis, but with the jet turned off or at greatly reduced power during the change of direction. Merritt & Ekers (2002) suggested another possible scenario, *i.e.* the reorientation of black holes’s spin axis due to a minor merger, leading to a sudden flip in the direction of any associated jet. A variant of Merritt & Ekers (2002) model was suggested by Gopal-Krishna, Biermann & Wiita (2003), where the sources with *Z* morphology within their *X*-shapes evolve along a *Z*–*X* morphological sequence. Presently, most of the observational results seem to pre-

^{*} E-mail: dharam@ncra.tifr.res.in

fer possibilities 3, 4 of Dennett-Thorpe et al. (2002) or Merritt & Ekers (2002), and the key difference between these two models is in terms of mechanism of reorientation; former favoured the disc instability mechanism because of little evidence for recent merger, while the latter preferred the coalescence scenario. Nevertheless, in all these scenarios, the wings are interpreted as relics of past radio jets and the active lobes as the newer ones.

Lal & Rao (2005) presented an unusual result for 3C 223.1 source, *i.e.* the wings (or low-surface-brightness jets) have flatter spectral indices with respect to the high-surface-brightness active lobes and this result is not easily explained in most models of the formation of *X*-shaped sources. Although unusual, it is a valuable result which puts stringent constraints on the formation models and nature of these sources. This unusual result for 3C 223.1 provides the motivation of this paper, *i.e.* systematic study of the sample of *X*-shaped sources using Giant Metrewave Radio Telescope (GMRT).

Furthermore, in the same paper, we presented an ‘alternative’ formation scenario, which was not addressed earlier, *i.e.* these sources consist of two pairs of jets, which are associated with two unresolved AGNs. We also presented some of the assumptions used in the spectral ageing method for estimating the age, in order to explain the unusual result. Briefly, these are as follows: (1) The injection spectral index is varying Palma et al. (2000). (2) In these sources, the low-surface-brightness, wings are in the process of becoming new active jets. Hence, it is not surprising that they have flatter spectral index compared to the active lobes. (3) Presence of some exotic reacceleration mechanism together with standard Alfvén waves and Fermi mechanisms. (4) There is a gradient in magnetic field across the source, together with a curved electron energy spectrum, which would result in spectral indices being different at distinct locations within the source (Blundell & Rawlings 2000).

We here present the GMRT results from a systematic study of the sample of *X*-shaped radio sources at 240 and 610 MHz. In Section 3, we describe the observations of the sample, data reduction (Section 4) and present the images derived from GMRT at 240 and 610 MHz along with distribution of low frequency, 240–610 MHz spectra across all these sources (Section 5). We also interpret our results, combine our data with previously published data for all of these sources, and discuss the statistical implications of these results on the formation models (Section 6). We summarize the salient conclusions of our study in Section 7.

2 SAMPLE

The sample is drawn from the list of *X*-shaped sources mentioned in Merritt & Ekers (2002) compiled by Leahy & Parma (1992). The sources have been selected solely on the basis of their morphology. 3C 192 was classified, as an *X*-shaped source Parma, Ekers & Fanti (1985), but was not included in the list of all such known sources (Merritt & Ekers 2002), and we have included it in our sample. However, it is important to note that the images on which the selection was based have been obtained with various instruments and with vast differences in sensitivity and resolution. Therefore, the sample of these twelve sources is

inhomogeneous and in no sense a statistical complete sample.

3 OBSERVATIONS

We adopted an observing strategy similar to our earlier observations for 3C 223.1 (Lal & Rao 2005). The 240 and 610 MHz feeds of GMRT are coaxial feeds and therefore, simultaneous dual frequency observations at these two frequencies were performed. The primary beams are $\sim 108'$ and $\sim 43'$ at 240 and 610 MHz, respectively. We made full synthesis observations of all the *X*-shaped sources 240 and 610 MHz, in the dual frequency mode, using the GMRT in the standard spectral line mode with a spectral resolution of 125 kHz. These sources were observed in two cycles (03DVL01: four of the eleven and 05DVL01: seven of the eleven sources). Table 1 gives the details of the observations. Since, NGC 326 is already observed using GMRT at low frequencies, we did not perform new observations.

The GMRT has a hybrid configuration (Swarup et al. 1991) with 14 of its 30 antennas located in a central compact array with size ~ 1.1 km and the remaining antennas distributed in a roughly ‘Y’ shaped configuration, giving a maximum baseline length of ~ 25 km. The baselines obtained from antennas in the central square are similar in length to the VLA *D*-array, while the baselines between the arm antennas are comparable in length to the VLA *B*-array. Hence, a single observation with the GMRT provides both, it samples the UV plane adequately on the short baselines as well as on the long baselines and provides good angular resolution when mapping the detailed source structure with reasonably good sensitivity.

4 DATA REDUCTION

The visibility data were converted to FITS and analyzed using standard AIPS. The flux calibrators 3C 48, 3C 147 and 3C 286 were observed depending on the availability either in the beginning and/or in the end as an amplitude calibrator and to estimate and correct for the bandpass shape. We used the flux density scale which is an extension of the Baars et al. (1977) scale to low frequencies, using the coefficients in AIPS task ‘SETJY’. The secondary phase calibrator were observed at intervals of 35 min. The error in the estimated flux density, both due to calibration and systematic, is $\lesssim 5\%$. The data suffered from scintillations and intermittent radio frequency interference (RFI). In addition to normal editing of the data, the scintillations affected data and channels affected due to RFI were identified and edited, after which the central channels were averaged using AIPS task ‘SPLAT’ to reduce the data volume. To avoid bandwidth smearing, effective band at 240 and 610 MHz was reduced to 5 and 3 channels, respectively.

While imaging, 49 facets spread across a $\sim 1.^\circ 8 \times 1.^\circ 8$ field were used at 240 MHz and 9 facets covering slightly less than a $0.^\circ 7 \times 0.^\circ 7$ field, were used at 610 MHz to map each of the two fields using AIPS task ‘IMAGR’. In order to achieve high resolution images that are also sensitive to extended structure, we have employed the SDI CLEANing algorithm (Steer, Dewdney & Ito 2003). We used ‘uniform’ weighting

Table 1. The observing log for all the observed X-shaped sources.

| | RA | Dec | Observing date | Bandwidth | | Centre frequency | Calibrator flux | Calibrator phase | $t_{\text{integration}}$ (on-source) (hour) |
|------------|------------|-------------|----------------|-----------|--------------|------------------|-----------------|----------------------|---|
| | (J2000) | | | Nominal | Effective | | | | |
| | | | | 610 MHz | / 240 MHz | | | | |
| 4C 12.03 | 00:09:52.6 | +12:44:04.9 | 18 Dec 2003 | 16/8 | 13.5/6 | 606.44/237.69 | 3C 286 | 0054–035 | 4.97 |
| 3C 52 | 01:48:29.0 | +53:32:35.4 | 12 Jan 2003 | 16/8 | 14.25/5 | 606.68/240.56 | 3C 286 | 0110+565 0114+483 | 6.29 |
| 3C 136.1 | 05:16:03.1 | +24:58:25.5 | 09 Jan 2003 | 16/8 | 14.25/6.75 | 606.68/240.06 | 3C 286 | 0521+166 | 5.65 |
| 3C 192 | 08:05:35.0 | +24:09:50.0 | 10 Apr 2004 | 16/6 | 13.125/5.625 | 606.31/240.19 | 3C 48 | 0804+102 | 6.38 |
| B2 0828+32 | 08:31:27.5 | +32:19:26.4 | 18 Dec 2003 | 16/8 | 13.125/5 | 606.31/236.44 | 3C 48 | 0909+428 | 6.94 |
| 3C 223.1 | 09:41:24.0 | +39:44:41.9 | 18 Dec 2003 | 16/8 | 14.25/5 | 606.68/237.19 | 3C 286 | 0834+555 | 6.67 |
| 4C 48.29 | 10:20:53.6 | +48:31:24.3 | 11 Apr 2004 | 16/6 | 13.875/5 | 606.44/240.12 | 3C 147 | 0834+555 | 6.42 |
| B1059+169 | 11:01:33.0 | +16:43:52.0 | 08 Feb 2004 | 16/8 | 13.5/6 | 606.25/240.06 | 3C 286 | 1021+219 | 5.33 |
| 3C 315 | 15:13:40.1 | +26:07:31.2 | 10 Jan 2003 | 8/6 | 6.375/5 | 610.13/237.19 | 3C 286 | 1506+375 | 5.89 |
| 3C 403 | 19:52:15.8 | +02:30:24.5 | 18 Dec 2003 | 16/8 | 13.5/6.25 | 606.37/236.94 | 3C 48 | 1941–154 | 4.97 |
| 3C 433 | 21:23:44.5 | +25:04:11.9 | 13 Jan 2003 | 8/6 | 6.375/5.625 | 610.13/240.75 | 3C 486 | 2225–049 2052+365 | 5.05 |

and the 3–D option for W term correction throughout our analysis. The presence of a large number of point sources in the field allowed us to do phase self-calibration to improve the image. After 2–3 rounds of phase self-calibration, a final self-calibration of both amplitude and phase was made to get the final image. At each round of self-calibration, the image and the visibilities were compared to check for the improvement in the source model. The final maps were combined using AIPS task ‘FLATN’ and corrected for the primary beam of the GMRT antennas.

5 RESULTS

The radio images shown in Figs. 1 to 11 have nearly complete UV coverage, an angular resolution $\sim 12''$ and $\sim 5''$ and the rms noise in the maps are in the range ~ 1.0 – 6.9 and ~ 0.2 – 0.8 mJy beam $^{-1}$ at 240 and 610 MHz, respectively. The dynamic ranges in the maps are in the range 900–2000 and 1700–5000 at 240 and 610 MHz, respectively. Consequently, in the vicinity of strong sources, including the sources discussed here, the local noise was sometimes higher than the noise in empty regions. The selection of contours shown in figures is based on the rms noise in the immediate vicinity of the source, with first contour level being 3–5 times this rms noise. To make further comparisons of the morphology and flux densities, the final calibrated UV data at 610 MHz was mapped using UV taper of 0–22 k λ , which is similar to that of 240 MHz data and then restored using the restoring beam corresponding to the 240 MHz map. The full synthesis 610 MHz, 240 MHz contour maps and the 610 MHz matched resolution contour map for all the observed sources are shown in Figs. 1 to 11. The sequence of maps is ordered in right ascension. An ellipse in a box in the lower left-hand corner of each map shows the shape of the synthesized beam (FWHM). All positions are given in J2000 coordinates.

5.1 Radio morphology and low frequency radio spectra

The first high angular resolution, high sensitivity images of X-shaped sources at the lowest frequencies of 240 MHz (upper right-hand panels) and 610 MHz (upper left-hand panels) are shown in Figs. 1 to 11. In all the sources, the radio morphologies at 240 and 610 MHz show well defined X-shape with a pair of active jets and a pair of wings, that pass symmetrically through the position of the parent galaxy. Table 2 list the integrated flux densities of all the sources along with previous measurements at other frequencies and are plotted in Fig. 12. Our estimates at both frequencies, 240 and 610 MHz agrees well with that of the measurements from other instruments. We therefore believe that we have not lost any flux density in our interferometric observations and there are no systematics introduced in our analysis.

The observations and morphologies described allow us to investigate in detail the spectral index distributions of all sources. The restored and matched maps at 240 and 610 MHz, were used further for the spectral analysis for each of these sources. We determine the spectral index distribution using the standard direct method of determining the spectral index between maps $S_{\nu_1}(x, y)$ and $S_{\nu_2}(x, y)$ at two frequencies ν_1 and ν_2 , and is given by the ratio of log $(S_{\nu_1}(x, y)/S_{\nu_2}(x, y))$ and log (ν_1/ν_2) .

The flux densities at 240 and 610 MHz plotted in Fig. 12 are calculated using the images shown in Figs. 1 to 11 (upper right-hand and lower left-hand panels), which are matched to the same resolution, and these values are tabulated in Tables 2 and 3. The flux densities for the active lobes and the wings are integrated over the region, which is at least four times the beam size (a circular region of ~ 5 pixels radius centered at the position of tail of the arrows shown using AIPS task ‘IMEAN’) and above their 3σ contour to reduce statistical errors. In addition, we have used conservative estimates of error-bars on the flux densities at each location. These estimates were determined from the fluctuations in the region being averaged and not from the noise at a source free location using similar sized circu-

Table 2. The total intensity for all the sources. The total flux densities quoted are in Jy along with corresponding error-bars (1σ). The 240 and 610 MHz are our GMRT measurements. The labels denote: ^aLarge Cambridge interferometer (Gower et al. 1967; Ryle 1960); ^bThe Molonglo reference catalogue of radio sources (Large et al. 1981); ^cGreen Bank, Northern Sky Survey (White & Becker 1992); ^dGregory & Condon (1991); ^eKellermann (1969); ^fKuhr et al. (1981); ^gLarge Cambridge interferometer (Pilkington & Scott 1965); ^hFicarra, Grueff & Tomassetti (1985); ⁱVLA FIRST survey (Becker, White & Helfand 1995); ^jGreen Bank, Northern Sky Survey (White & Becker 1992; Becker, White & Edwards 1991).

| | 178 MHz | 240 MHz | 408 MHz | 610 MHz | 1400 MHz | 2695 MHz | 4850 MHz |
|------------|------------------|------------------|--------------------|------------------|--------------------|-------------------|-------------------|
| 4C 12.03 | 7.6 ± 1.0^a | 6.62 ± 0.12 | 4.45 ± 0.20^b | 2.94 ± 0.05 | 2.01 ± 0.10^c | | 0.54 ± 0.07^d |
| 3C 52 | 13.7 ± 1.1^a | 11.71 ± 0.68 | | 6.44 ± 0.40 | 3.80 ± 0.19^e | 2.30 ± 0.12^e | 1.55 ± 0.17^d |
| 3C 136.1 | 14.0 ± 2.1^e | 10.41 ± 0.05 | | 5.76 ± 0.03 | 2.90 ± 0.44^e | 2.08 ± 0.10^e | 0.56 ± 0.75^d |
| 3C 192 | 21.0 ± 3.2^e | 20.51 ± 0.28 | 11.03 ± 0.90^f | 9.08 ± 0.12 | 4.80 ± 0.20^f | 3.23 ± 0.16^f | 2.68 ± 0.10^f |
| B2 0828+32 | | 7.17 ± 0.05 | | 2.23 ± 0.02 | 2.07 ± 0.10^c | | 0.44 ± 0.06^d |
| 3C 223.1 | 8.7 ± 1.1^g | 8.33 ± 0.41 | 4.72 ± 0.10^h | 3.56 ± 0.17 | 1.90 ± 0.28^i | 1.23 ± 0.61^e | 0.78 ± 0.11^j |
| 4C 48.29 | 4.5 ± 0.6^a | 5.73 ± 0.04 | | 2.56 ± 0.03 | | | 0.35 ± 0.04^d |
| B1059+169 | | 1.61 ± 0.02 | 1.02 ± 0.22^b | 0.80 ± 0.01 | 0.62 ± 0.10^c | | 0.21 ± 0.03^d |
| 3C 315 | 20.3 ± 1.7^f | 39.83 ± 0.33 | 10.62 ± 0.87^f | 8.95 ± 0.09 | 4.10 ± 0.20^f | 2.39 ± 0.05^f | 1.28 ± 0.17^d |
| 3C 403 | 30.9 ± 4.0^f | 17.62 ± 0.72 | 13.57 ± 0.59^b | 9.81 ± 0.38 | 6.05 ± 0.19^f | 3.65 ± 0.18^f | 2.06 ± 0.10^f |
| 3C 433 | 60.4 ± 4.8^f | 57.75 ± 3.98 | 29.26 ± 2.30^f | 20.59 ± 1.21 | 12.40 ± 0.35^f | 6.63 ± 0.33^f | 4.05 ± 0.54^d |

lar region, which being much smaller (see Fig. captions). These error-bars, both spectral indices and flux densities, do not change significantly with increasing or decreasing the size of circle, and they also do not change significantly by changing slightly the position of circular region. Furthermore, we have also examined the possibility that (i) the different UV coverages, (ii) the negative depression around the source and (iii) the image misalignments at 240 and 610 MHz could produce some systematic errors. The former seems unlikely since the GMRT has good UV coverage, and sources are only $\sim 3'-4'$ across and are much smaller than the short baseline lengths, $\sim 35'$ ($\simeq 100$ wavelengths) at 610 MHz and $\sim 100'$ ($\simeq 35$ wavelengths) at 240 MHz. Nevertheless, we Fourier transform the 240 MHz CLEAN map, sampling it with the UV coverage of 610 MHz and re-imaging this visibility data set. The resultant map showed no systematic differences from the original 240 MHz map and the rms difference in the two maps was less than 4%, corresponding to the rms error in the spectral index of $\lesssim 0.05$. Furthermore, 240 MHz maps of two sources (Fig. 6: 3C 223.1 and Fig. 11: 3C 433) show marginal evidence that these images contain a negative depression around them. Negative depression/bowl is seen in a synthesis image, either due to inadequate UV coverage at short baseline lengths or due to inadequate CLEANing. The former is unlikely as explained above, examining the latter—While imaging, we did not provide zero-spacing flux density, but we have done deep CLEANing, so as not to make any deconvolution errors. Comparisons of expected integrated flux density, total CLEANed flux density and flux density measured by short baseline lengths suggest no discrepancy beyond 5%. In any case, we quantify the errors that would be introduced due to possible negative depression for these two sources below. Finally, in each case, we not only registered the target source, the positions of at least five field sources around the X-shaped source, which were common in the two maps were also registered, and the two images alignment is better than 15%. Therefore, in order to understand the nature of X-shaped sources, we take into account our

careful analyses and estimation of the possible systematic errors.

Analysis of the spectrum, shown in Figs. 1 to 11 (lower right-hand panels), in different regions of each of these sources show remarkable variation across them. The lighter regions represent the relatively steep spectrum as compared to the darker regions which represent flat spectrum. Although the full range of spectral index is large, we have shown only small range for clarity in each case. We now describe the radio structure of X-shaped radio sources measured by the GMRT, along with the best power-law fit ($S_\nu \propto \nu^\alpha$) for several regions across the source. Here, we also include the description of 3C 223.1 (Lal & Rao 2005) and NGC 326 (Murgia et al. 2001), published in the literature.

NGC 326 ($z = 0.047$)

The galaxy is the brightest member of the Zwicky cluster 0056.9+2636 (Zwicky & Kowal 1968). The host is a dumbbell shaped galaxy with clearly separated nuclei (Wirth, Smarr & Gallagher 1982).

NGC 326 was the first X-shaped radio source discovered (Ekers et al. 1978). At 1.4 GHz, the lobes are slightly resolved and the most prominent components are the two wings. The lobes are asymmetric in total emission, extent and distance from the core. The southern lobe has an ellipsoidal shape, while the northern lobe is more elongated and wider (Murgia et al. 2001). The wings bend and extend away from the lobe axis by $\sim 2''$. Furthermore, the overall Z-shape symmetry is broken by the low-surface-brightness plume located just above the end of the east wing (Worrall, Birkinshaw & Cameron 1995).

In the east wing there is monotonic steepening of the radio spectrum from the south lobe to the end of the wing; the spectral index distributions between 1.4 and 4.8 GHz and between 4.8 and 8.5 GHz decrease from -0.6 and -0.7 up to -1.3 and -1.9 , respectively. Whereas in the west wing,

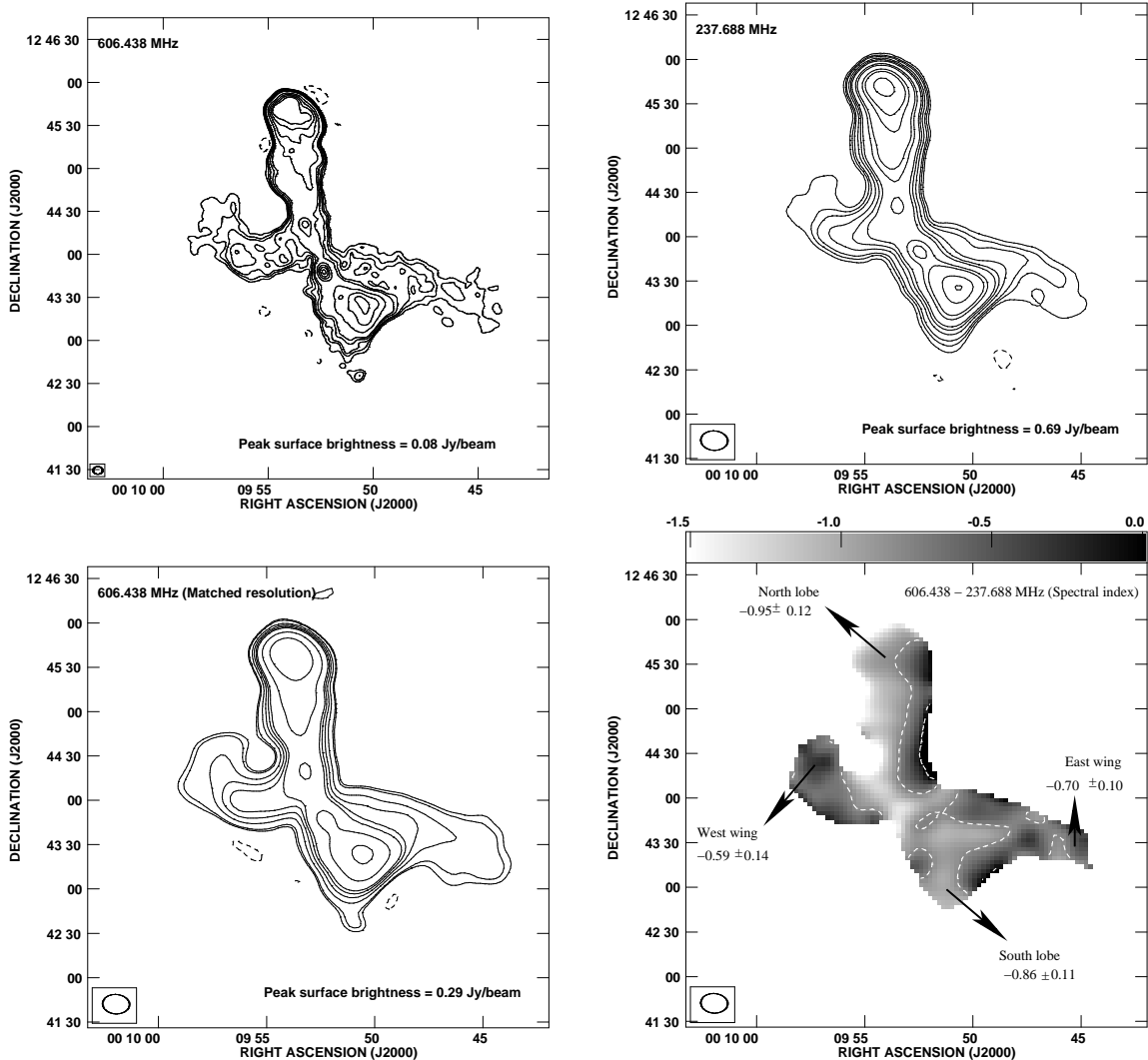


Figure 1. Upper: Full synthesis GMRT maps of 4C 12.03 at 610 (left panel) and 240 MHz (right panel). The CLEAN beams for 610 and 240 MHz maps are $6''.7 \times 5''.5$ at a P.A. of $89^\circ.8$ and $18''.2 \times 13''.1$ at a P.A. of $86^\circ.4$, respectively; and the contour levels in the two maps, respectively are $-2, 2, 3, 4, 6, 8, 16, 24, 32, 40$ mJy beam^{-1} and $-20, 20, 30, 40, 60, 80, 100, 160, 200, 320, 400$ mJy beam^{-1} . Lower left: The map of 4C 12.03 at 610 MHz matched with the resolution of 240 MHz. The contour levels are $-6, 6, 8, 16, 24, 32, 40, 80, 160$ mJy beam^{-1} . Lower right: The distribution of the spectral index, between 240 and 610 MHz, for the source. The spectral index contours are at $-0.8, 0$. The error-bars in the full synthesis maps found at a source free location are ~ 2.0 and ~ 0.3 mJy beam^{-1} at 240 and 610 MHz, respectively.

the spectral index distributions between 1.4 and 4.8 GHz and between 4.8 and 8.5 GHz decrease, respectively from -0.6 and -0.7 up to -1.3 and -1.5 (Murgia et al. 2001). Similarly, in the south lobe the spectral index distribution between 1.4 and 4.8 GHz is roughly constant around a value of 0.6 and the spectral index distribution between 4.8 and 8.5 GHz decreases from -0.7 to -1.3 . Whereas in the north lobe the spectral index distributions between 1.4 and 4.8 GHz and between 4.8 and 8.5 GHz increase, respectively from -0.75 and -1.35 at the lobe head, to -0.65 and -0.8 and becomes -1.0 and -1.6 in proximity of the core (Murgia et al. 2001). Briefly, the active lobes have flatter 1.4–8.5 GHz spectral index as compared to the wings and the 0.325–1.4 GHz spectra also shows similar behaviour (private communication).

4C 12.03 ($z = 0.110$)

4C 12.03 is associated with an elliptical host galaxy (Heckman et al. 1994) and has been classified as a low emission line radio galaxy (Laing, Riley & Longair 1983). Morphologically, 4C 12.03 seems to lie at the FR I/FR II division, whereas the radio luminosity suggests it to be a FR I source.

Fig. 1 at 240 and 610 MHz shows symmetrical structure and extent in the two matched resolution radio maps, as is usually the case for radio galaxies. The northern jet leading to north hot spot possibly consists of the active axis and the other axis, *i.e.* the east-west axis consists of the wings. The source has an angular extent of $3.8' \times 4.0'$ in both, 240 and 610 MHz maps.

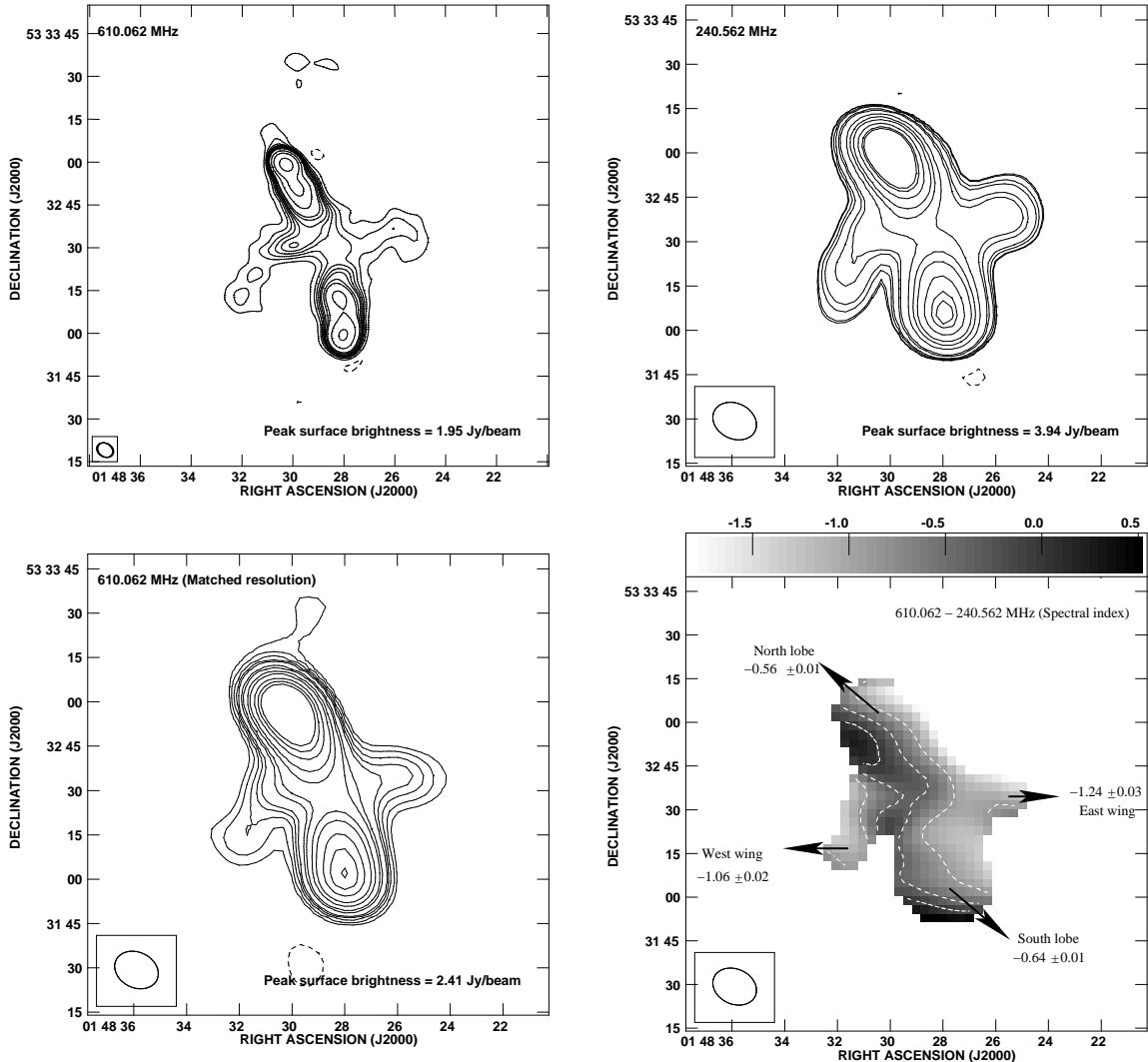


Figure 2. Upper: Full synthesis GMRT maps of 3C 52 at 610 (left panel) and 240 MHz (right panel). The CLEAN beams for 610 and 240 MHz maps are $5''.9 \times 4''.7$ at a P.A. of $57^\circ.5$ and $15''.4 \times 12''.0$ at a P.A. of $63^\circ.7$, respectively; and the contour levels in the two maps, respectively are $-8, 8, 20, 30, 40, 50, 60, 80, 100, 200$ mJy beam^{-1} and $-50, 50, 60, 80, 100, 160, 200, 400, 600, 800, 1200, 1600, 1800$ mJy beam^{-1} . Lower left: The map of 3C 52 at 610 MHz matched with the resolution of 240 MHz. The contour levels are $-24, 24, 40, 60, 80, 100, 160, 200, 300, 400, 600, 800$ mJy beam^{-1} . Lower right: The distribution of the spectral index, between 240 and 610 MHz, for the source. The spectral index contours are at $-0.9, -0.4, 0$. The error-bars in the full synthesis maps found at a source free location are ~ 1.4 and ~ 0.3 mJy beam^{-1} at 240 and 610 MHz, respectively.

The high frequency spectral index distribution between 1.5 and 10.45 GHz at a resolution of $69'' \times 69''$ shows marginal steepening from the active lobes ($\alpha \simeq -0.8$) to the wings ($\alpha \simeq -1.0$) (Rottmann 2001). The low frequency fitted spectra have $-0.59 > \alpha > -0.95$ for all regions across the source. Contrary to the high frequency spectral results, the low frequency result shows definite evidence for steeper spectra in the active lobes than in the wings, and the east and west wings have spectral indices, -0.70 ± 0.10 and -0.59 ± 0.14 , respectively, whereas the north and south active lobes have -0.95 ± 0.12 and -0.86 ± 0.11 , respectively.

3C 52 ($z = 0.285$)

3C 52 is the most distant X-shaped source. *HST* imaging by de Koff (1996) showed the galaxy to be elongated along the north-south axis and it shows a pronounced dust disk.

Fig. 2 shows the radio images at 240 and 610 MHz. The core is undetected in low resolution radio maps, but closer inspection of radio contours in the 610 MHz map shows presence of possible core at the position of parent galaxy. Historically, this source is an example of a mirror symmetric distortion, but it is now described by rotational symmetry (Leahy & Williams 1984).

High frequency spectral index constructed at a resolution of $5''.0 \times 4''.8$ using images at 1.4, 1.7 and 2.7 GHz show indication for a spectral steepening towards the wings

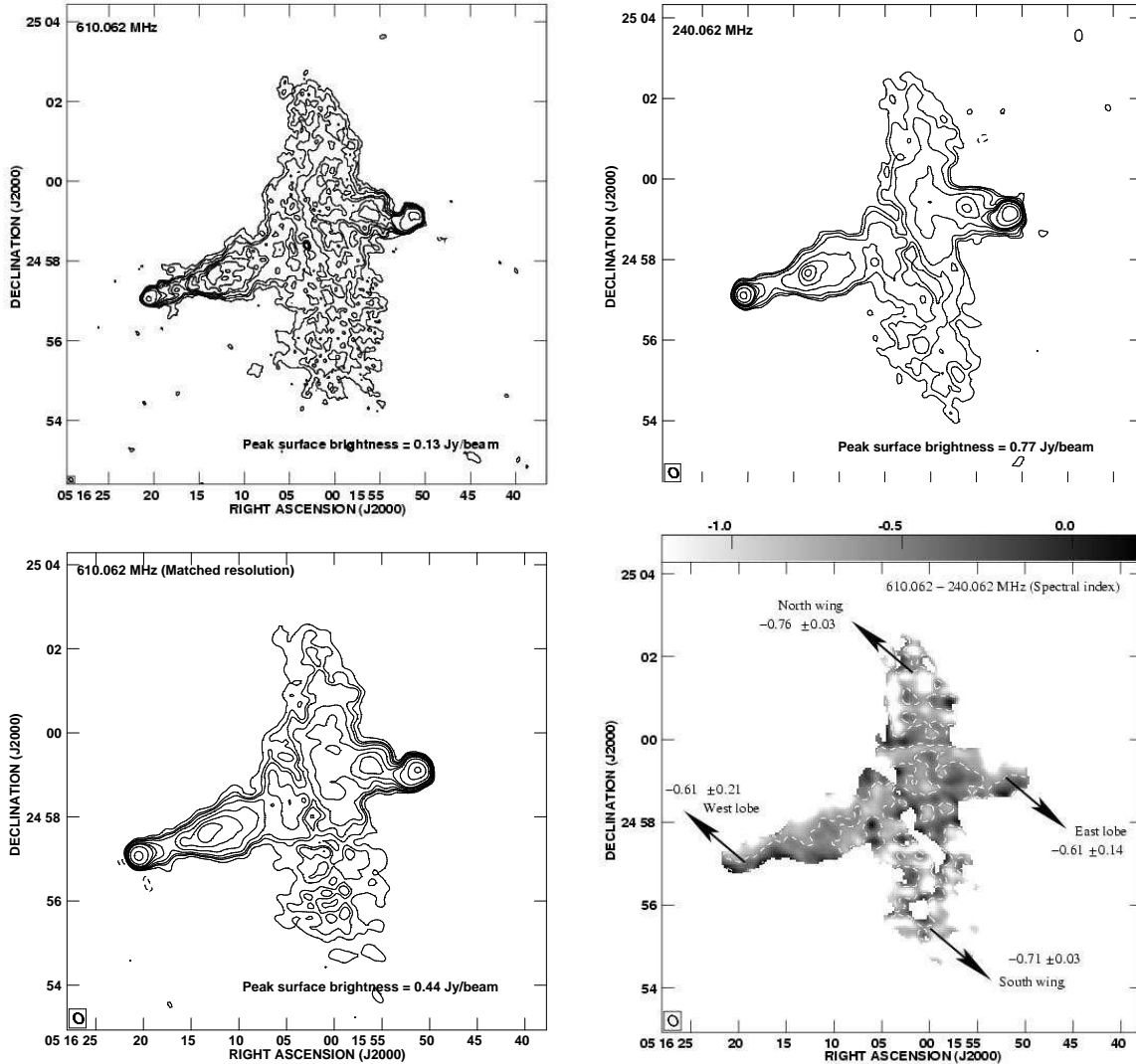


Figure 3. Upper: Full synthesis GMRT maps of 3C 136.1 at 610 (left panel) and 240 MHz (right panel). The CLEAN beams for 610 and 240 MHz maps are $6''.7 \times 5''.1$ at a P.A. of $28^\circ.2$ and $15''.5 \times 12''.3$ at a P.A. of $32^\circ.7$, respectively; and the contour levels in the two maps, respectively are $-1.6, 1.6, 2.4, 3.2, 4.8, 6, 8, 10, 20, 80$ mJy beam $^{-1}$ and $-8, 8, 12, 20, 40, 60, 80, 100, 200, 400$ mJy beam $^{-1}$. Lower left: The map of 3C 136.1 at 610 MHz matched with the resolution of 240 MHz. The contour levels are $-3, 3, 6, 8, 12, 20, 30, 40, 80, 200, 400$ mJy beam $^{-1}$. Lower right: The distribution of the spectral index, between 240 and 610 MHz, for the source. The spectral index contours are at $-0.6, 0.2$. The error-bars in the full synthesis maps found at a source free location are ~ 1.2 and ~ 0.2 mJy beam $^{-1}$ at 240 and 610 MHz, respectively. The white patches in the spectral index map seen in the wings are steep spectrum features and is due to slightly higher noise cut-off.

(Rottmann 2001). Author also finds prominent spectral steepening from the south lobe towards the west wing as compared to mild spectral steepening from the north lobe towards the east wing. Similar spectral steepening between 1.4 and 5.0 GHz from south lobe towards the east wing and from north lobe towards the west wing was also found by Alexander & Leahy (1987) The low frequency fitted spectra have $-0.56 > \alpha > -1.24$ for all regions across the source. The source shows evidence for flatter spectra in the active lobes than in the wings. The east and west wings have spectral indices, -1.24 ± 0.03 and -1.06 ± 0.02 , respectively, whereas the north and south active lobes have -0.56 ± 0.01 and -0.64 ± 0.01 , respectively.

3C 136.1 ($z = 0.064$)

It is a low galactic latitude object in the sample. *HST* image of the host galaxy (Martel et al. 1999) shows flattened and warped host and bears no resemblance with an elliptical galaxy. The host galaxy possibly has two/three nuclei and seems to be showing irregular, disrupted, possibly by tidal forces, signs of on-going merger.

Fig. 3 shows the radio images at 240 and 610 MHz, maps show similar extent and morphology along both axes, similar to its radio map at high frequency (Leahy & Williams 1984). Therefore their suggestion that some of the large-scale structure may be missing from their map is unlikely. The core is

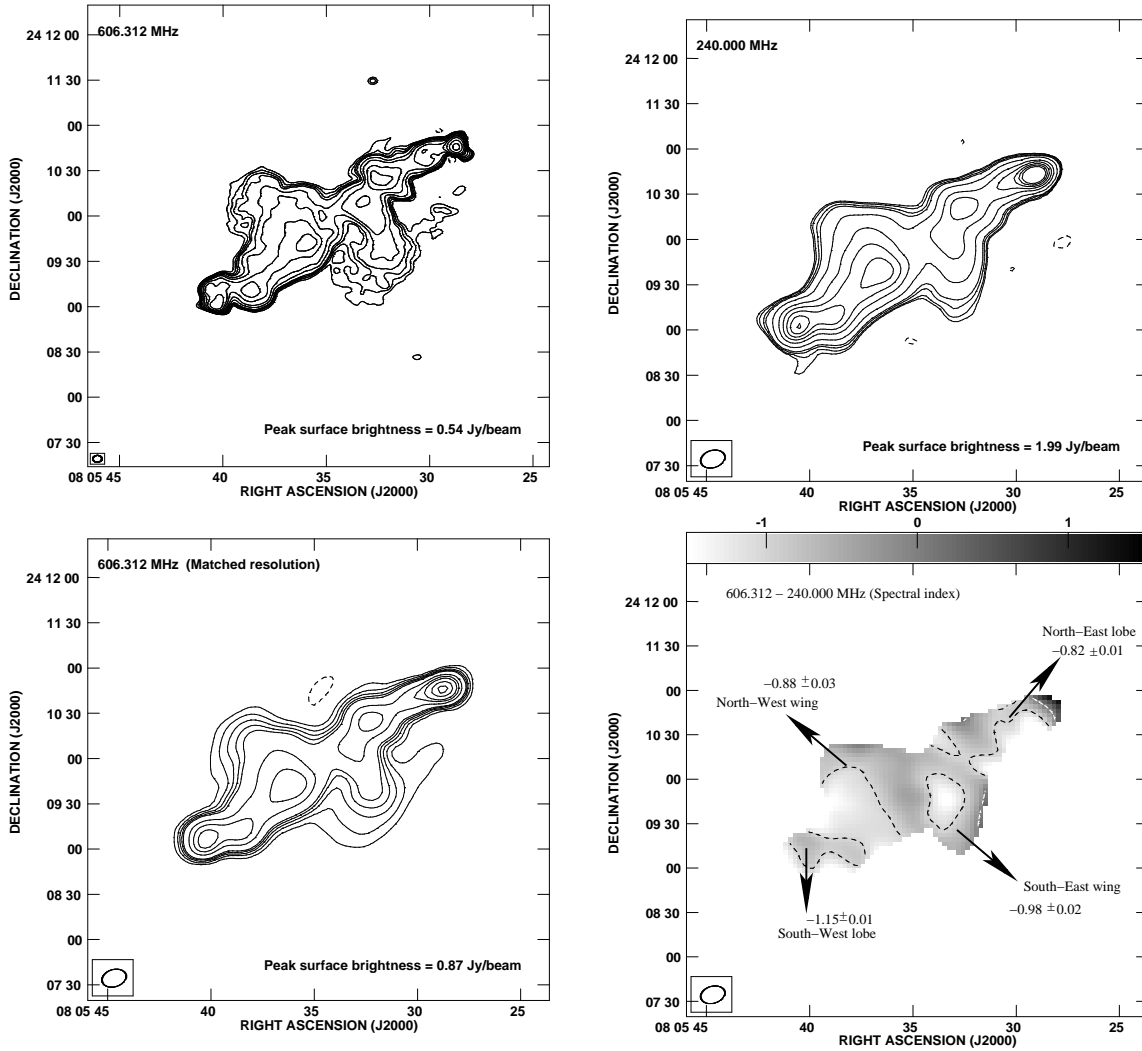


Figure 4. Upper: Full synthesis GMRT maps of 3C 192 at 610 (left panel) and 240 MHz (right panel). The CLEAN beams for 610 and 240 MHz maps are $6''.0 \times 4''.5$ at a P.A. of $-88^\circ.1$ and $16''.5 \times 11''.5$ at a P.A. of $-73^\circ.2$, respectively; and the contour levels in the two maps, respectively are $-4, 4, 6, 8, 10, 16, 24, 40, 60, 80, 100, 200, 400, 600, 800, 1000$ mJy beam $^{-1}$ and $-50, 50, 60, 80, 100, 200, 400, 600, 800, 1000$ mJy beam $^{-1}$. Lower left: The map of 3C 192 at 610 MHz matched with the resolution of 240 MHz. The contour levels are $-20, 20, 40, 60, 80, 100, 200, 300, 400, 600, 800, 1000$ mJy beam $^{-1}$. Lower right: The distribution of the spectral index, between 240 and 610 MHz, for the source. The spectral index contours are at $-1, 0$. The error-bars in the full synthesis maps found at a source free location are ~ 2.4 and ~ 0.5 mJy beam $^{-1}$ at 240 and 610 MHz, respectively.

clearly detected in 610 MHz maps and is marginally detected in 240 MHz map.

The spectral index maps of 3C 136.1 using radio maps at 1.37, 4.85 and 10.45 GHz at resolutions of $69'' \times 69''$ and $147'' \times 147''$ show a spectral gradient from the active lobes ($-0.50 > \alpha > -0.65$) towards the wings (Rottmann 2001). The spectral gradient is more pronounced along the east lobe ($\alpha = -0.6$) to the south wing ($\alpha = -1.0$) as compared to the spectral gradient along the west lobe ($\alpha = -0.7$) to the north wing ($\alpha = -0.85$). Alexander & Leahy (1987) also found spectral steepening between 1.4 and 5.0 GHz from west lobe towards the core and from east lobe towards the north wing using VLA and Cambridge 5 km telescope. The low frequency fitted spectra have $-0.61 > \alpha > -0.76$ for all regions across the source. Similar to the high frequency result, our result also shows evidence for steeper spectra in

the wings than in the active lobes and the north and south wings have spectral indices, -0.76 ± 0.03 and -0.71 ± 0.03 , respectively, whereas the east and west active lobes have -0.61 ± 0.14 and -0.61 ± 0.21 , respectively.

3C 192 ($z = 0.060$)

3C 192 was classified, as a X-shaped source having prominent distorted structure of rotational type (Parma, Ekers & Fanti 1985).

Fig. 4 shows the radio images at 240 and 610 MHz. The angular extents along the active axis and the wings are $\sim 210''$ and $\sim 120''$, respectively at both frequencies. Both the maps show similar radio extent along the active axis and along the wings, consistent with earlier work (Högbom 1979;

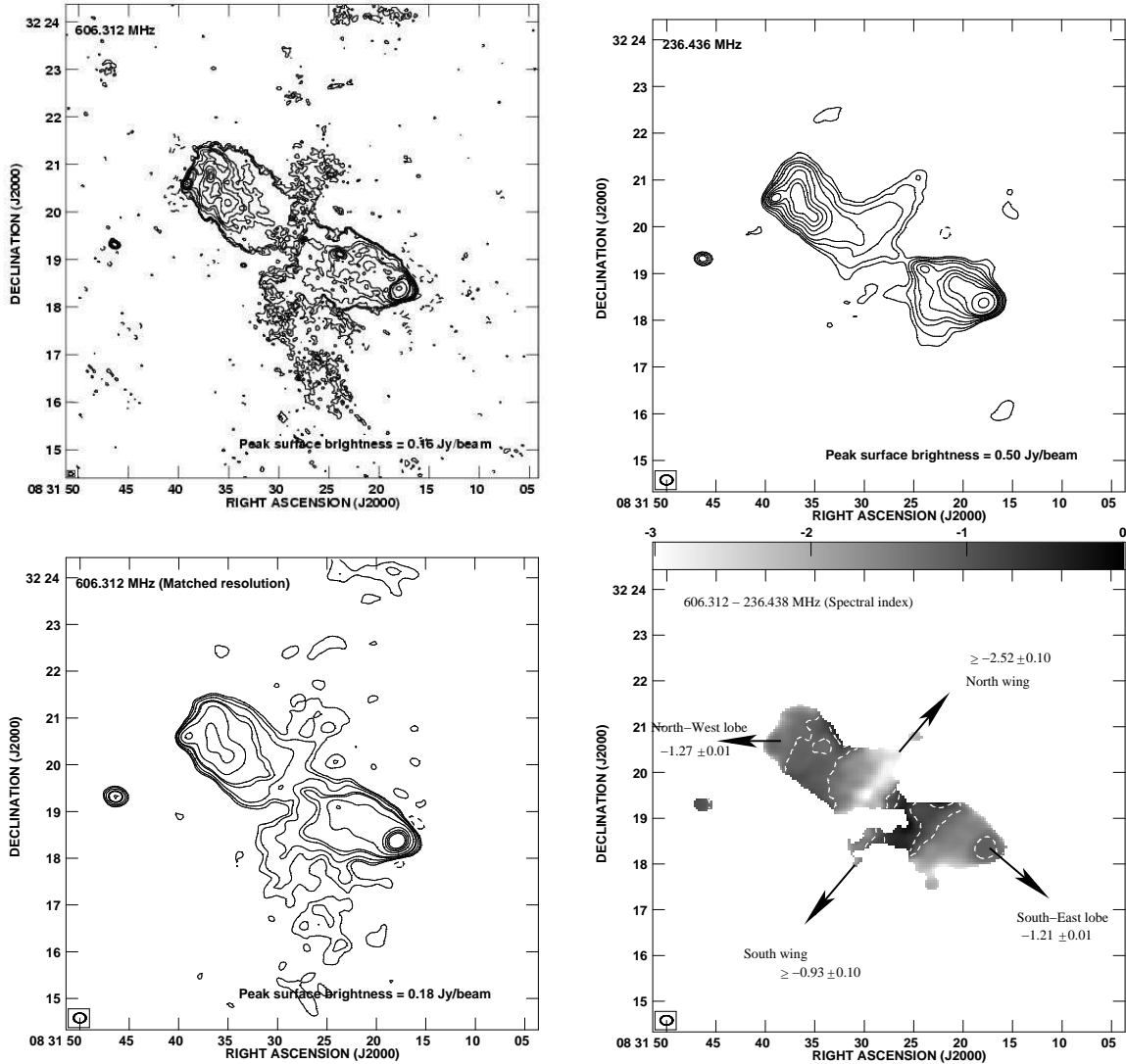


Figure 5. Upper: Full synthesis GMRT maps of B2 0828+28 at 610 (left panel) and 240 MHz (right panel). The CLEAN beams for 610 and 240 MHz maps are $6''.0 \times 4''.8$ at a P.A. of $81^\circ.9$ and $15''.8 \times 12''.5$ at a P.A. of $89^\circ.2$, respectively; and the contour levels in the two maps, respectively are $-1, 1, 2, 3, 4, 6, 8, 10, 20, 40$ mJy beam^{-1} and $-14, 14, 20, 30, 40, 50, 80, 100, 120, 200, 400$ mJy beam^{-1} . Lower left: The map of B2 0828+28 at 610 MHz matched with the resolution of 240 MHz. The contour levels are $-1, 1, 2, 4, 8, 10, 20, 30, 40, 60, 80, 100$ mJy beam^{-1} . Lower right: The distribution of the spectral index, between 240 and 610 MHz, for the source. The spectral index contours are at $-1.2, -0.7, 0$. The error-bars in the full synthesis maps found at a source free location are ~ 2.7 and ~ 0.2 mJy beam^{-1} at 240 and 610 MHz, respectively.

Dennett-Thorpe et al. 1999), and both the wings have symmetrical distortions. The radio structure in the central parts of this source is confused, but the detailed shape of the contours close to the position of the host galaxy clearly indicates the presence of a weak unresolved central component. There is also a weak transverse feature across the south-east wing.

The low frequency fitted spectra have $-0.82 > \alpha > -1.15$ for all regions across the source. The source shows evidence for comparable spectra in the active lobes than in the wings. The north-west and south-east wings have spectral indices, -0.88 ± 0.03 and -0.98 ± 0.02 , respectively, whereas the north-east and south-west active lobes have -0.82 ± 0.01 and -1.15 ± 0.01 , respectively.

B2 0828+32 ($z = 0.053$)

B2 0828+32 is the most extended X-shaped source in the sample. Although, the host galaxy neither have a double core nor a companion, the luminosity profile shows faint possibility of a merger event (Ulrich & Rönnback 1996).

Fig. 5 shows the radio images at 240 and 610 MHz. The source shows large scale ‘S’ type distortions, suggestive of precession phenomenon of the central engine (Parma, Ekers & Fanti 1985). The south-east–north-west axis consists of prominent hot spots, which is possibly the active axis; whereas the north-south axis is along the wings, which is barely visible in our maps and in our low resolution ($30'' \times 30''$) maps. The faint detection of hot spot is likely in our 610 MHz map and not in our low resolution

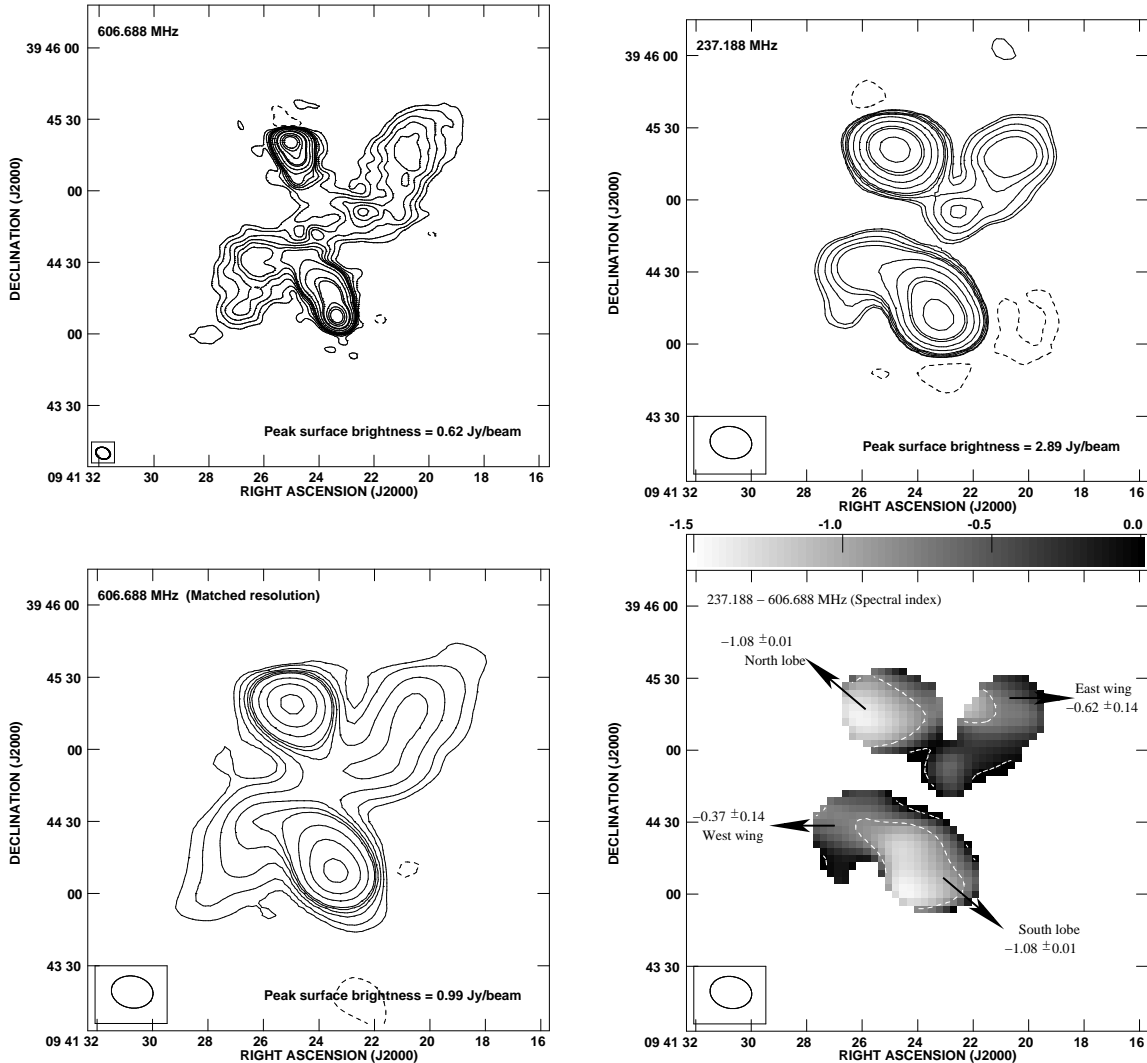


Figure 6. Upper: Full synthesis GMRT maps of 3C 223.1 at 610 (left panel) and 240 MHz (right panel). The CLEAN beams for 610 and 240 MHz maps are $6''.1 \times 4''.8$ at a P.A. of $66^\circ.8$ and $17''.4 \times 13''.3$ at a P.A. of $80^\circ.3$, respectively; and the contour levels in the two maps, respectively are $-2, 2, 4, 6, 8, 10, 12, 20, 40, 80, 100, 200, 300, 400 \text{ mJy beam}^{-1}$ and $-32, 32, 60, 80, 100, 200, 400, 800, 1000, 4000 \text{ mJy beam}^{-1}$. Lower left: The map of 3C 223.1 at 610 MHz matched with the resolution of 240 MHz. The contour levels are $-10, 10, 20, 40, 60, 80, 100, 200, 400, 800, 1000 \text{ mJy beam}^{-1}$. Lower right: The distribution of the spectral index, between 240 and 610 MHz, for the source. The spectral index contours are at $-0.8, 0$. The error-bars in the full synthesis maps found at a source free location are ~ 3.0 and $\sim 0.4 \text{ mJy beam}^{-1}$ at 240 and 610 MHz, respectively.

maps, which were earlier detected in high resolution images at 1.4 and 5 GHz. (Parma, Ekers & Fanti 1985; Feretti et al. 1983). This is one of the first X-shaped source, identified as two double radio structures of different ages and oriented at widely different angles (Ulrich & Rönnback 1996).

The high frequency spectral index (1.4–10.55 GHz) exhibits gradual steepening from the active lobes ($\alpha \simeq -0.7$) towards the wings ($\alpha \simeq -1.1$, southern wing and $\alpha \simeq -1.1$, northern wing) (Rottmann 2001). The low frequency fitted spectra have $-0.37 \geq \alpha \geq -2.79$ for all regions across the source. Even though the radio maps and the spectral index map are rather noisy, due mainly to the absence of the north wing and the south wing in our 240 MHz map, there is a weak evidence for steeper spectra in the active lobes than in the wings. The spectral index of the north wing is flatter

than $\geq -2.79 \pm 0.30$ and of the south wing is steeper than $\leq -0.37 \pm 0.21$. Instead, the north-west and south-east active lobes have spectral indices of -1.27 ± 0.01 and -1.21 ± 0.01 , respectively.

3C 223.1 ($z = 0.108$)

The host galaxy was imaged as part of the *HST* snapshot survey (de Koff 1996) and the galaxy has a strong central bulge and a very pronounced dust disk. The source is believed to be isolated or in a poor group (Sandage 1972) and no X-ray emission was detected from it or at its surroundings (Burns, Gregory & Holman 1981).

Fig. 6 shows complex radio source with an X-shaped morphology at both 240 and 610 MHz. The angular extent

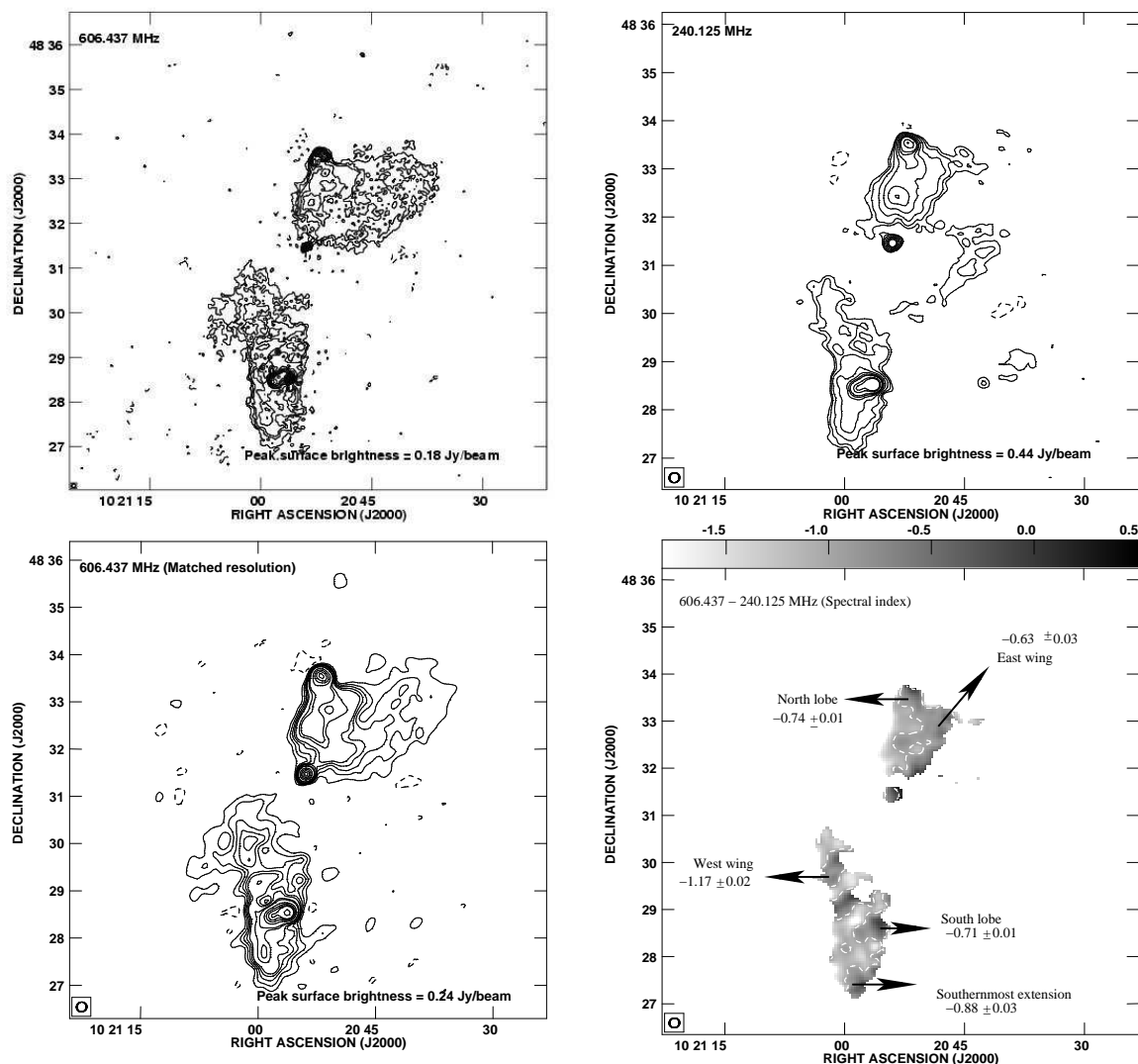


Figure 7. Upper: Full synthesis GMRT maps of 4C 48.29 at 610 (left panel) and 240 MHz maps are $5''.1 \times 5''.0$ at a P.A. of $-65^\circ.3$ and $12''.6 \times 12''.2$ at a P.A. of $-48^\circ.9$, respectively; and the contour levels in the two maps, respectively are $-0.8, 0.8, 1, 2, 3, 4, 5, 6, 8, 10, 40$ mJy beam^{-1} and $-12, 12, 16, 24, 40, 60, 80, 100, 160, 200$ mJy beam^{-1} . Lower left: The map of 4C 48.29 at 610 MHz matched with the resolution of 240 MHz. The contour levels are $-2, 2, 4, 6, 8, 10, 16, 20, 40, 60, 80, 100$ mJy beam^{-1} . Lower right: The distribution of the spectral index, between 240 and 610 MHz, for the source. The spectral index contours are at $-1, 0$. The error-bars in the full synthesis maps found at a source free location are ~ 2.6 and ~ 0.2 mJy beam^{-1} at 240 and 610 MHz, respectively.

is $\sim 105''$ along the active lobes (those with hot-spots) and $\sim 150''$ along the wings. The nuclear source of 3C 223.1 is invisible at both these frequencies and also in the radio maps of Dennett-Thorpe et al. (2002), but is detected and is unresolved at 8.4 GHz (Black et al. 1992). The weak jet detected mid-way between core and north lobe at 8.4 GHz (Black et al. 1992) is not seen in our maps, because of coarser resolution. Our maps also suggest of a sharp boundary at the farthest end of the north lobe and a likely ring-like feature in the south lobe, which is consistent with earlier results.

The low frequency fitted spectra have $-0.37 > \alpha > -1.08$ for all regions across the source, and is the first X-shaped source showing evidence for steeper spectra in the active lobes than in the wings (Lal & Rao 2005). Here, we do

look into the errors that would be introduced due to possible negative depression. The maximum depression close to the source at 240 and 610 MHz are -7.6 and -2.7 mJy beam^{-1} respectively. This worst case would introduce a maximum error of 0.14 in spectral indices for the wings and 0.01 for the active lobes. The east and west wings have spectral indices, -0.37 ± 0.14 and -0.62 ± 0.14 , respectively, whereas the north and south active lobes have -1.08 ± 0.01 and -1.08 ± 0.01 , respectively, and are consistent with spectral results between 1.4 and 32 GHz, *i.e.* -0.70 ± 0.03 and -0.66 ± 0.03 for the east and west wings, and -0.75 ± 0.02 and -0.77 ± 0.02 for the north and south active lobes, respectively (Dennett-Thorpe et al. 2002). Since, the observed differences in spectral index at low frequencies are much more than the uncertainties, we believe that the observed spectral

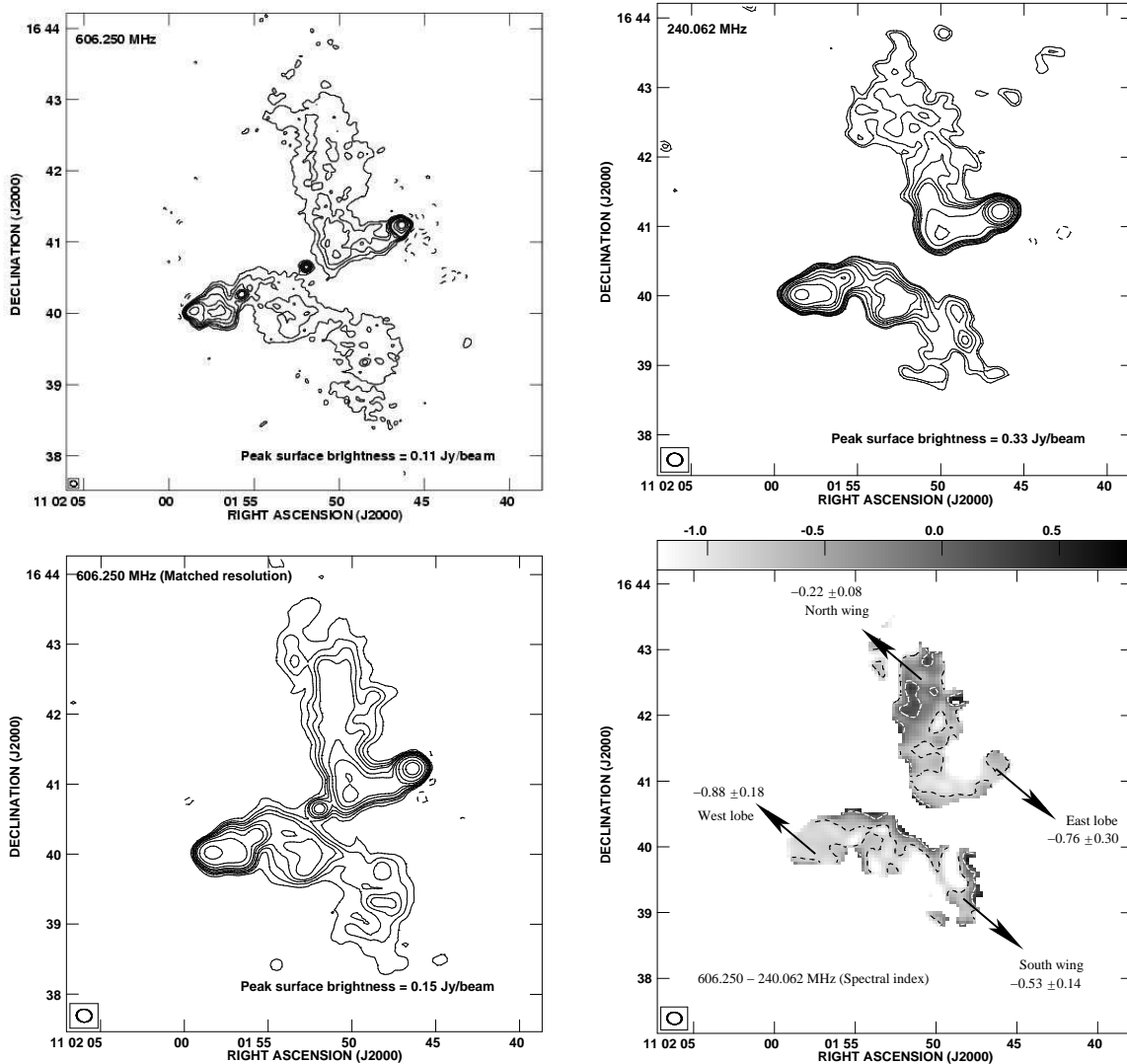


Figure 8. Upper: Full synthesis GMRT maps of B1059+169 at 610 (left panel) and 240 MHz (right panel). The CLEAN beams for 610 and 240 MHz maps are $5''.7 \times 4''.9$ at a P.A. of $77^\circ.0$ and $13''.0 \times 11''.1$ at a P.A. of $82^\circ.5$, respectively; and the contour levels in the two maps, respectively are $-1, 1, 2, 4, 6, 8, 16, 24, 32$ mJy beam^{-1} and $-3, 3, 4, 6, 8, 10, 12, 20, 30, 40, 60, 100$ mJy beam^{-1} . Lower left: The map of B1059+169 at 610 MHz matched with the resolution of 240 MHz. The contour levels are $-1, 1, 2, 3, 4, 6, 8, 12, 20, 40, 60$ mJy beam^{-1} . Lower right: The distribution of the spectral index, between 240 and 610 MHz, for the source. The spectral index contours are at $-0.8, 0$. The error-bars in the full synthesis maps found at a source free location are ~ 1.0 and ~ 0.2 mJy beam^{-1} at 240 and 610 MHz, respectively.

index features are real. Similar result, ‘spectral reversal’ was also found independently by Rottmann (2001).

4C 48.29 ($z = 0.053$)

This source is the nearest to us and is at the centre of Abell 990 cluster. The parent galaxy belongs to a double system with no visible companion on the Palomar Sky Survey (PSS) prints (Parma, Ekers & Fanti 1985), but a companion is detected, $\sim 25''$ away on the south-east on the 2 Metre All Sky Survey (2MASS), which is probably a starburst galaxy.

Fig. 7 shows the radio images at 240 and 610 MHz and they show that the brightest components of the hot spots are well aligned with the core, which is consistent with the

results of van Breugel & Jägers (1982). The source has a peculiar X-shaped morphology, with an additional, wing like feature at the south of the south active lobe. Furthermore, 240 MHz map shows a low surface brightness feature $\sim 2'$ to the east and a point source $\sim 4'$ to the south-east of the core.

The low frequency fitted spectra have $-0.63 > \alpha > -1.17$ for all regions across the source. The east and west wings have spectral indices, -0.63 ± 0.03 and -1.17 ± 0.02 , respectively, whereas the north and south active lobes have -0.74 ± 0.01 and -0.71 ± 0.01 , respectively. Furthermore, the southernmost extension has a spectral index of -0.88 ± 0.03 . Briefly, the east wing definitely shows evidence for flatter spectra than either of the two active lobes; otherwise rest of the regions have comparable spectral indices.

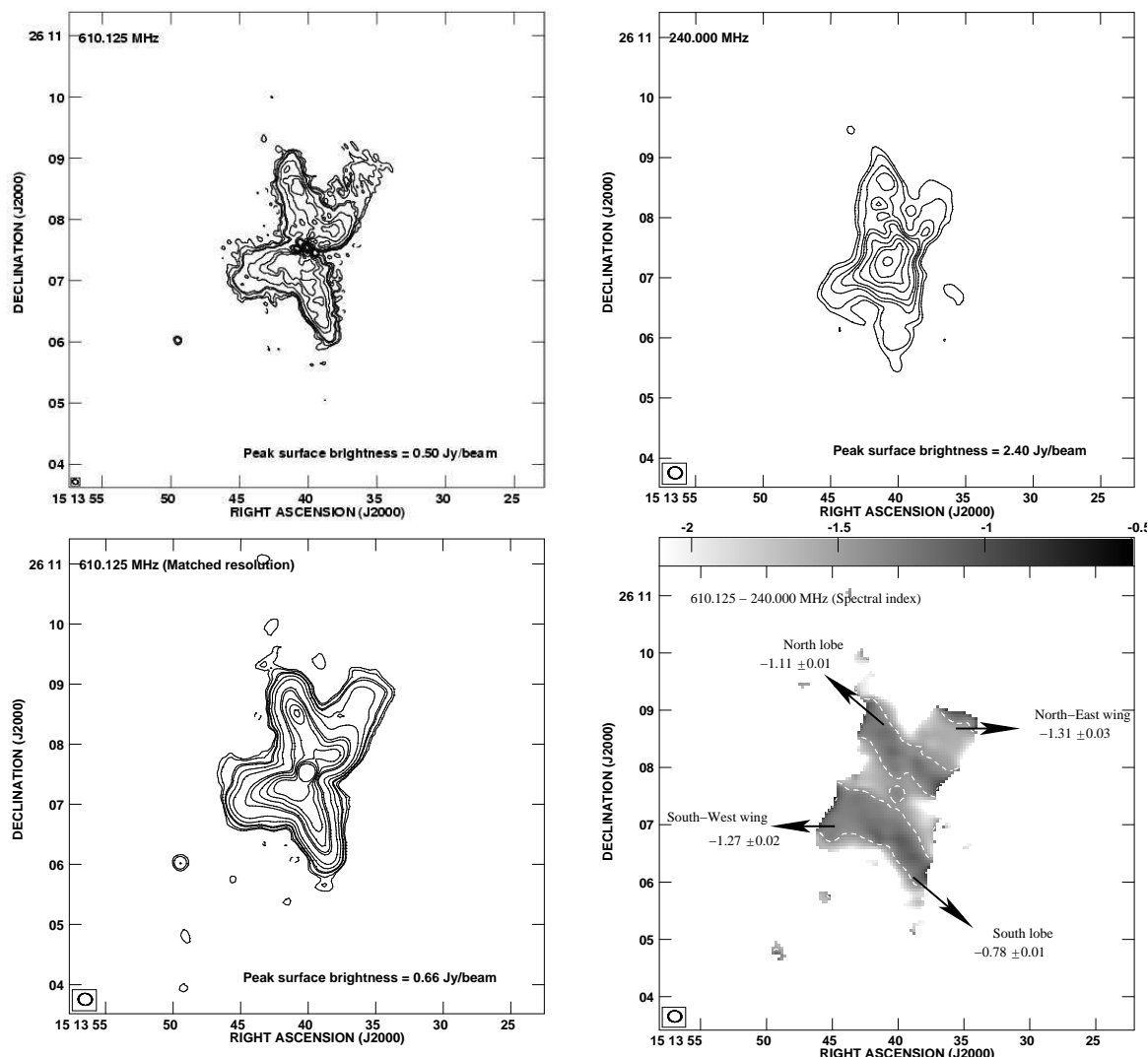


Figure 9. Upper: Full synthesis GMRT maps of 3C 315 at 610 (left panel) and 240 MHz (right panel). The CLEAN beams for 610 and 240 MHz maps are $5''.7 \times 4''.7$ at a P.A. of $62^\circ.0$ and $13''.6 \times 11''.8$ at a P.A. of $84^\circ.1$, respectively; and the contour levels in the two maps, respectively are $-2, 2, 4, 8, 20, 30, 40, 80, 100, 200, 400, 800$ mJy beam $^{-1}$ and $-160, 160, 240, 400, 500, 600, 800, 1000, 1200, 2000$ mJy beam $^{-1}$. Lower left: The map of 3C 315 at 610 MHz matched with the resolution of 240 MHz. The contour levels are $-3, 3, 4, 8, 10, 20, 40, 100, 120, 160, 200, 240, 300$ mJy beam $^{-1}$. Lower right: The distribution of the spectral index, between 240 and 610 MHz, for the source. The spectral index contours are at $-1.7, 0.5$. The error-bars in the full synthesis maps found at a source free location are ~ 6.8 and ~ 0.3 mJy beam $^{-1}$ at 240 and 610 MHz, respectively.

B1059+169 ($z = 0.068$)

B1059+169 is the another source seen in cluster environment (Abell 1145), which is the dominant radio galaxy and is $\sim 5.5'$ away from the cluster centre. A companion is detected on the 2MASS, coincident with the cluster centre.

The morphology at low frequency (Fig. 8) is similar to the 1.4 GHz map of Owen & Ledlow (1997). The extent of the east-west active axis is $200'$ in both the maps, whereas the extent of the north-south axis in 240 MHz map is $310'$, which is slightly more than the extent of the wings in the 610 MHz map. This could be possibly due to spectral ageing, which is a common phenomenon for head-tail and wide-angle-tail radio sources, seen in clusters, exhibit-

ing low-surface-brightness features. In the 610 MHz map, we also detect a knot inbetween the west lobe and the core.

The low frequency fitted spectra have $-0.22 > \alpha > -0.88$ for all regions across the source. Although *B1059+169* is found in the cluster environment, surprisingly, the spectral results of it are similar to that of 4C 12.03 and 3C 223.1, *i.e.* the wings have relatively flatter spectral index as compared to the active lobes. The north and south wings have spectral indices, -0.22 ± 0.08 and -0.53 ± 0.14 , respectively, whereas the east and west active lobes have -0.76 ± 0.30 and -0.88 ± 0.18 , respectively. Furthermore, the knot inbetween the west lobe and the core has a spectral index of -0.82 ± 0.22 , similar to the east and west active lobes.

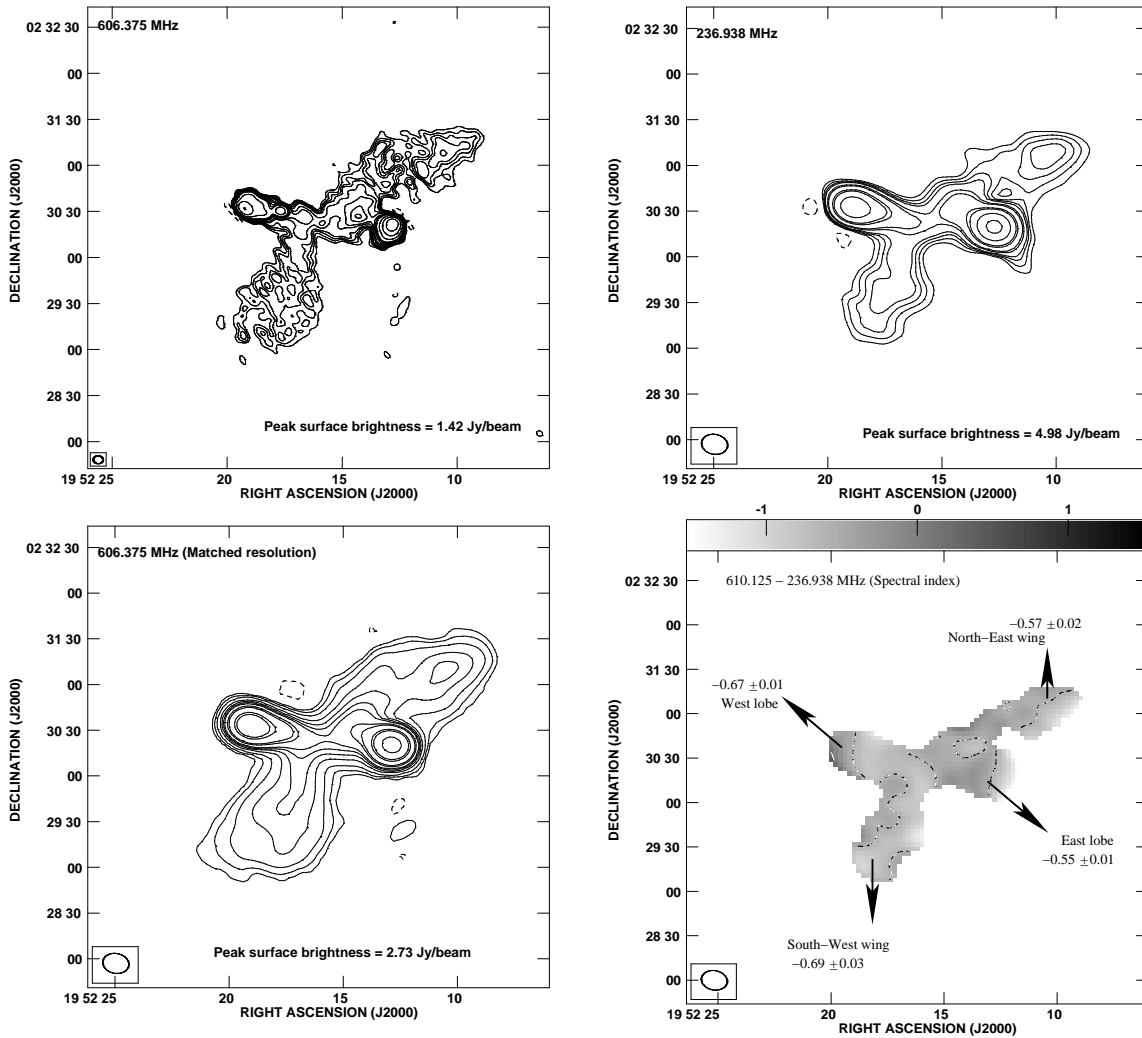


Figure 10. Upper: Full synthesis GMRT maps of 3C 403 at 610 (left panel) and 240 MHz (right panel). The CLEAN beams for 610 and 240 MHz maps are $6''.4 \times 5''.1$ at a P.A. of $85^\circ.3$ and $17''.3 \times 13''.1$ at a P.A. of $79^\circ.0$, respectively; and the contour levels in the two maps, respectively are $-8, 8, 12, 16, 20, 30, 40, 60, 80, 100, 200, 400, 800$ mJy beam $^{-1}$ and $-80, 80, 120, 160, 200, 320, 400, 800, 1000$ mJy beam $^{-1}$. Lower left: The map of 3C 403 at 610 MHz matched with the resolution of 240 MHz. The contour levels are $-10, 10, 20, 40, 80, 120, 160, 200, 320, 400, 800, 1000$ mJy beam $^{-1}$. Lower right: The distribution of the spectral index, between 240 and 610 MHz, for the source. The spectral index contours are at $-0.6, 0.2$. The error-bars in the full synthesis maps found at a source free location are ~ 4.8 and ~ 0.5 mJy beam $^{-1}$ at 240 and 610 MHz, respectively.

3C 315 ($z = 0.108$)

Similar to NGC 326 and 4C 48.29, here also, the host galaxy belongs to a double system with no visible companion on the PSS prints (Parma, Ekers & Fanti 1985), but $\sim 7''$ away on the south, a companion is detected on the 2MASS, and is identified to be a irregular galaxy. Their optical profiles show signs of interaction and seems to be located in a poor cluster (Zirbel 1997). *HST* image of the northern core, containing the radio source shows an elliptical host (de Koff 1996).

Fig. 9 shows the radio images at 240 and 610 MHz with both the axes to be roughly of similar angular sizes and surface brightnesses, making it a very unusual source (Alexander & Leahy 1987). But, as suggested by Högbom (1979), the jet along the north-south axis being of slightly higher surface brightness and could define a recent axis of activity. The core is clearly detected in both the radio maps

and is associated with the brightest member of a pair of elliptical galaxy (Leahy & Williams 1984). Furthermore, the source does not display characteristic elongated structure, *i.e.* the usual hot spots at or near the extreme edges.

The spectral index map of 3C 315 using the radio maps at 1.65 and 2.7 GHz at a resolution of $9.1'' \times 5.5''$ shows relatively flat spectral index regions close to the core and steep spectral index regions being located at the tips of the active lobes. The southern and northern active lobes have high frequency (1.65–2.7 GHz) spectral indices, -1.46 and -1.26 , respectively (Rottmann 2001). The low frequency fitted spectra have $-0.78 > \alpha > -1.31$ for all regions across the source, and shows evidence for flatter spectra in the active lobes than in the wings. The north-east and south-west wings have spectral indices, -1.31 ± 0.03 and -1.27 ± 0.02 , respectively, whereas the north and south active lobes

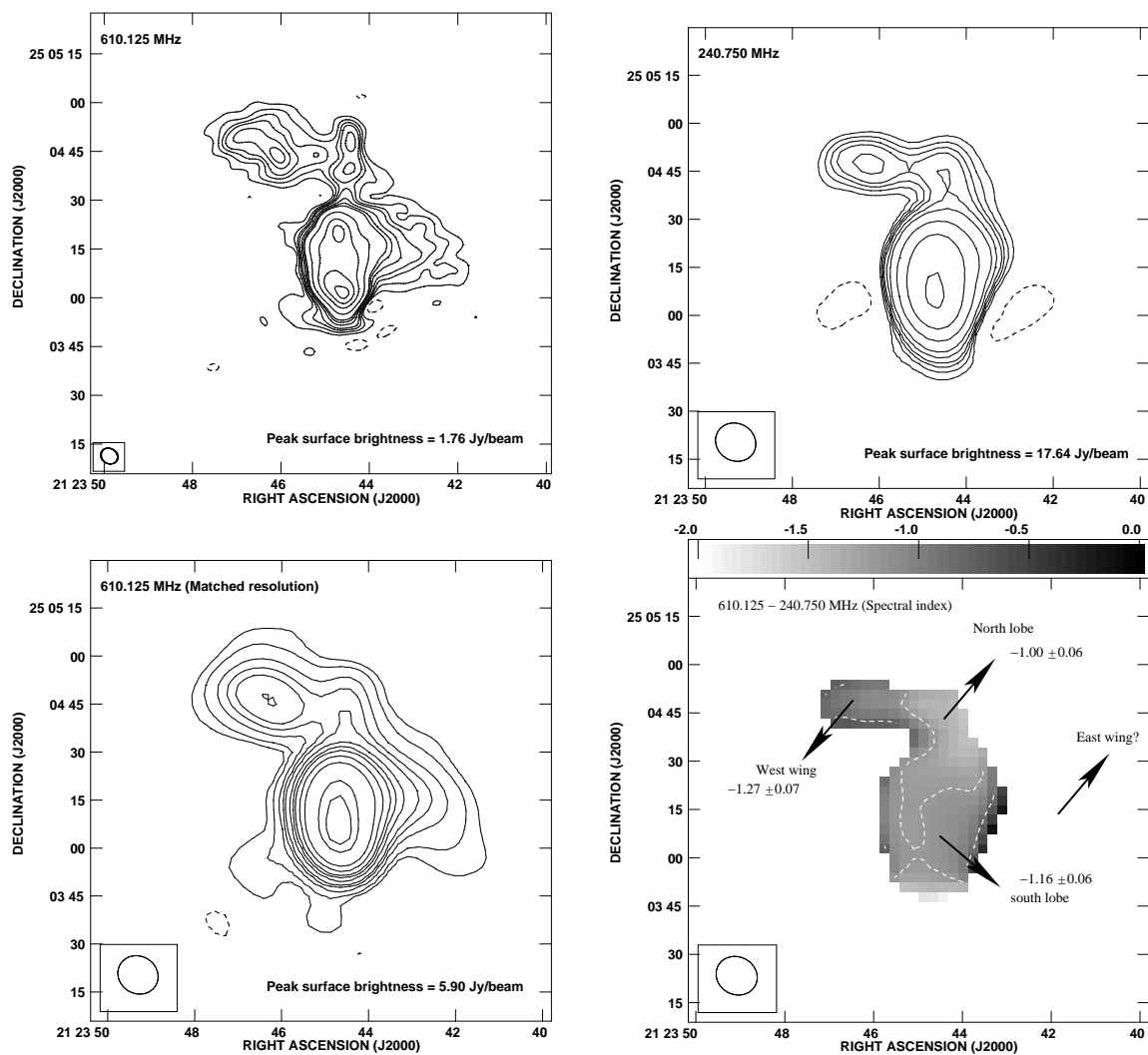


Figure 11. Upper: Full synthesis GMRT maps of 3C 433 at 610 (left panel) and 240 MHz (right panel). The CLEAN beams for 610 and 240 MHz maps are $5''.4 \times 4''.6$ at a P.A. of $57^\circ.9$ and $12''.9 \times 11''.6$ at a P.A. of $58^\circ.7$, respectively; and the contour levels in the two maps, respectively are $-20, 20, 40, 60, 80, 120, 160, 200, 400, 800, 1200$ mJy beam $^{-1}$ and $-400, 400, 600, 800, 1000, 1400, 2000, 4000, 8000$ mJy beam $^{-1}$. Lower left: The map of 3C 433 at 610 MHz matched with the resolution of 240 MHz. The contour levels are $-50, 50, 100, 200, 300, 400, 600, 800, 1000, 1400, 2000, 4000$ mJy beam $^{-1}$. Lower right: The distribution of the spectral index, between 240 and 610 MHz, for the source. The spectral index contours are at $-1.2, -0.8, 0$. The error-bars in the full synthesis maps found at a source free location are ~ 6.9 and ~ 0.8 mJy beam $^{-1}$ at 240 and 610 MHz, respectively.

have -1.11 ± 0.01 and -0.78 ± 0.01 , respectively. The spectral index map (Fig. 9, lower right panel) shows peculiar spectral behaviour and are consistent with the findings of Alexander & Leahy (1987) and Rottmann (2001), *i.e.* the spectrum is steep at the wings, it becomes flatter in regions close to the core, and again steepens towards the active lobe and ultimately becomes steepest at the tip of the active lobes.

3C 403 ($z = 0.059$)

The host of 3C 403 is a E0, narrow-line radio galaxy (NED classification) and the continuum colors are typical of an early type galaxy. The galaxy appears to be a smooth elliptical using *HST* with an apparent separation of the source into

a central elliptical region and a low-surface-brightness halo, which is probably due to intervening dust (Martel et al. 1999). The host galaxy does not have any bright companion and is located in a very low-density local galaxy environment (Heckman et al. 1994).

Fig. 10 shows the radio images at 240 and 610 MHz, and the east and west hot spots are clearly detected. The slightly larger angular extent of the north-south axis along the wings in 240 MHz map than in 610 MHz and high frequency maps (Dennett-Thorpe et al. 1999) could be due to spectral ageing.

The low frequency fitted spectra have $-0.55 > \alpha > -0.69$ for all regions across the source. The south-west and north-east wings have spectral indices, -0.69 ± 0.03 and -0.57 ± 0.02 , respectively, whereas the east and west active lobes have -0.55 ± 0.01 and -0.67 ± 0.01 , respec-

tively. These results are inconsistent with results at high frequency (Dennett-Thorpe et al. 2002; Rottmann 2001), *i.e.* the spectral indices between 1.4 and 32 GHz are -0.80 ± 0.03 and -0.77 ± 0.28 for the south-west and north-east wings, respectively, (note that Dennett-Thorpe et al. 2002 label the south-west and north-east wings as the south-east and north-west wings, respectively), and -0.78 ± 0.02 and -0.77 ± 0.02 for the east and west active lobes, respectively. Instead, the source shows evidence for comparable spectra in the active lobes and the wings.

3C 433 ($z = 0.102$)

The host has a disturbed morphology (PSS prints) with no known nearby companion and lies in a cluster (McCarthy, Spinard & van Breugel 1995). *HST* image the source shows galaxy full of filaments of dust, a faint patch of emission north-west of the galaxy coinciding with a spot of radio emission and possible regions of star formation (de Koff 1996).

Fig. 11 shows the radio images at 240 and 610 MHz. Since, our map at 240 MHz is a low resolution map, therefore several features seen in van Breugel et al. (1983) and Black et al. (1992) are smoothed, and it is unclear if the source is indeed X-shaped source. Instead, the 610 MHz map shows many of the features to be clearly resolved similar to the VLA map at 6 cm (van Breugel et al. 1983; Black et al. 1992). We clearly detect weak, collimated emission to the north from the lobe forming, A, B and C (for the positions of A to I, see Fig. 1(a) of van Breugel et al. 1983). The eastern feature, D is also clearly detected. As suggested by van Breugel et al. (1983), the south lobe seem to flare out close to the nucleus with a relatively large opening angle forming the eastern jet along I. We define regions centered at B and H to be the north and south active lobes, respectively, and we believe that the two lobes do not appear to be relaxed systems. The low-surface-brightness regions centered at D and I, respectively, are assumed to be the east and west wings for our further analysis.

We do not detect the east wing in our low frequency map and the fitted spectra have $-1.00 > \alpha \geq -3.42$ for all regions across the source. The source shows marginal evidence for comparable spectra in the active lobes and the wings. The west wing has spectral index, -1.27 ± 0.03 and the east wing is flatter than $\geq -3.42 \pm 0.21$, whereas the north and south active lobes have -1.00 ± 0.03 and -1.16 ± 0.01 , respectively. Here again, we quantify the errors introduced due to possible negative depression, being -94.2 and -10.1 mJy beam $^{-1}$ at 240 and 610 MHz respectively, close to the source; thereby introducing a maximum error of 0.07 in spectral indices for the wings and 0.06 for the active lobes, which are smaller than the quoted statistical errors.

6 DISCUSSION

The low frequency GMRT observations combined with observations at other wavelengths raise a number of questions regarding the nature and the formation scenario of the X-shaped sources. Some of the earlier scenarios that were based on limited information need to be investigated. In this section we first, discuss the overall source morphological and

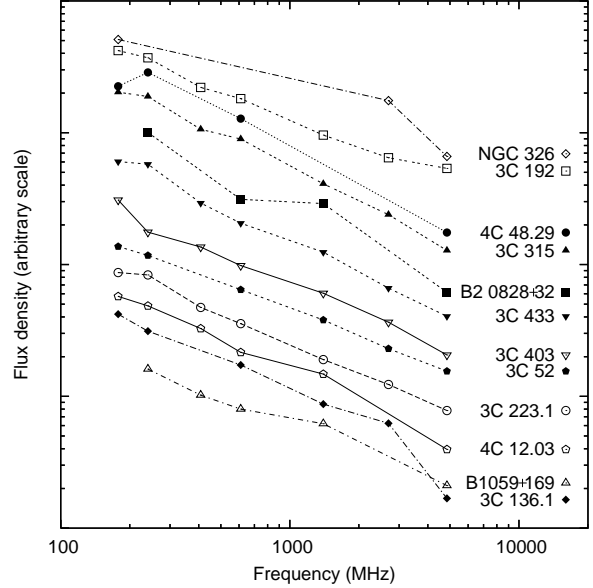


Figure 12. Integrated flux density (spectra) for the sample of X-shaped sources. Various measurements along with the error-bars (not plotted) are explained in Table 2. The spectra are shifted with respect to one another for clarity.

spectral properties (Section 6.1). We then weigh all the *pros* and *cons* of existing models (Section 6.2), and statistical implications of these results on our understanding of the current formation models for the known sample of X-shaped sources (Section 6.3). Finally, in Section 6.4, we address the question, do X-shaped sources constitute a single class in the light of ‘merger of two AGNs’ model.

6.1 Overall source properties

Nearly a dozen sources have been mapped in detail, with a resolution approaching to ~ 1 kpc in most cases. Here, a few qualitative points about the overall source morphological and spectral properties, based on images presented are made.

6.1.1 Source morphological properties

The salient features of morphology of all X-shaped sources are as follows:

(i) Almost all sources show similar angular sizes for the two axes. Marginal differences between two axes in 3C 192 and 3C 403, can be attributed to the projection effects.

(ii) Source 3C 315 have all four lobes of almost similar surface brightness, thereby making difficult to identify the active lobes and the wings.

(iii) Although, 3C 433 is classified as X-shaped source, it does not have ‘typical’ ‘X’ shape morphology. It also is the source with smallest angular size in the sample.

(iv) The radio core is detected for only one of the source, B1059+169 in its 610 MHz map. Whereas the radio maps of sources, 4C12.03, 4C 48.29 and 3C 315 at 610 MHz show marginal detection of the radio cores.

Table 3. Flux densities of all the distinct regions at 240 and 610 MHz. The error-bars for these sources are quoted in the respective figure captions. Label denotes: †The upper limits on the flux densities quoted are five times the rms noise levels.

| | | Flux density | |
|------------|-----------------|--------------------|-------------------|
| | | 240 MHz | 610 MHz |
| | | (mJy) | |
| 4C 12.03 | North lobe | 2214.9 | 915.0 |
| | South lobe | 1376.3 | 618.9 |
| | East wing | 117.5 | 67.8 |
| | West wing | 91.5 | 47.6 |
| 3C 52 | North lobe | 5312.0 | 3035.9 |
| | South lobe | 2395.0 | 1314.4 |
| | East wing | 384.0 | 121.2 |
| | West wing | 272.6 | 101.8 |
| 3C 136.1 | East lobe | 904.0 | 511.3 |
| | West lobe | 2149.0 | 1214.6 |
| | North wing | 163.5 | 80.2 |
| | South wing | 159.5 | 82.4 |
| 3C 192 | North-East lobe | 383.2 | 167.9 |
| | South-West lobe | 478.7 | 192.0 |
| | South-East wing | 2351.3 | 1091.5 |
| | North-West wing | 2405.8 | 824.8 |
| B2 0828+32 | South-East lobe | 1288.8 | 416.8 |
| | North-West lobe | 1213.4 | 372.0 |
| | North wing | <13.5 [†] | <1.0 [†] |
| | South wing | <13.5 [†] | 19.1 |
| 3C 223.1 | North lobe | 2946.1 | 1074.9 |
| | South lobe | 3268.6 | 1196.7 |
| | East wing | 123.8 | 87.8 |
| | West wing | 175.5 | 98.3 |
| 4C 48.29 | North lobe | 462.2 | 232.3 |
| | South lobe | 689.7 | 356.8 |
| | East wing | 51.9 | 28.9 |
| | West wing | 98.9 | 33.2 |
| | Southernmost | 251.5 | 110.4 |
| B1059+169 | East lobe | 210.3 | 92.4 |
| | West lobe | 226.7 | 111.6 |
| | North wing | 25.9 | 21.0 |
| | South wing | 23.5 | 14.4 |
| 3C 315 | North lobe | 1140.6 | 403.6 |
| | South lobe | 938.2 | 453.7 |
| | North-East wing | 1018.3 | 300.6 |
| | South-West wing | 977.5 | 291.7 |
| 3C 403 | East lobe | 5856.9 | 3133.0 |
| | West lobe | 3740.9 | 2241.7 |
| | North wing | 512.1 | 300.1 |
| | South wing | 549.5 | 287.9 |
| 3C 433 | North lobe | 1685.3 | 663.5 |
| | South lobe | 21025.0 | 7066.3 |
| | East wing | <34.0 [†] | 831.1 |
| | West wing | 1530.8 | 467.0 |

(v) Hot spots are almost always detected in the high-surface-brightness active lobes in both, 610 and 240 MHz radio maps.

(vi) We detect the high-surface-brightness jets in almost, in fact all the X-shaped sources and this nearly 100%, high rate of jet detection is similar to Leahy et al. (1997) and Hardcastle et al. (1997) for classical radio sources.

6.1.2 Global spectral morphological properties

The integrated radio flux densities at several locations across each of these sources, allow us to group them into following three categories: (A) Sources in which the wings are of flatter spectral indices than the active lobes, *i.e.* 4C 12.03, 3C 223.1 and B1059+169. These sources have spectral indices, $-0.22 > \alpha_{\text{wings}} > -0.70$ and $-0.76 > \alpha_{\text{active lobes}} > -1.08$ for all regions across the source. In addition, in the former two sources, the wings (or low-surface-brightness jets) have flatter spectral indices with respect to the high-surface-brightness jets at high radio frequencies (Dennett-Thorpe et al. 2002; Rottmann 2001), consistent with our low frequency results. (B) Sources in which the wings and the active lobes have comparable spectral indices, *i.e.* 3C 192, B2 0828+32, 4C 48.29 and 3C 403. Here, these classes of sources have spectral indices, $-0.37 \geq \alpha_{\text{wings}} \geq -2.79$ and $-0.55 > \alpha_{\text{active lobes}} > -1.27$ for all regions across the source. It therefore seems that although the two regions, the wings and the active lobes, have comparable spectral indices, they are relatively flat as compared to typical steep spectrum features. It is important to note, since we have limits for spectral indices of the north and south wings, we have included B2 0828+32 in this category, although the south wing seems to be flatter than the active lobes. (C) Sources in which the wings are of steeper spectral indices as compared to the active lobes, *i.e.* NGC 326, 3C 52, 3C 136.1, 3C 315 and 3C 433. This category of sources have spectral indices, $-0.71 > \alpha_{\text{wings}} \geq -3.42$ and $-0.56 > \alpha_{\text{active lobes}} > -1.16$ for all regions across the source. This latter class of sources are similar to typical radio galaxies, where low-surface-brightness features have steeper spectral indices as compared to the high-surface-brightness features, which have relatively flat spectral indices. The result of the former two classes of sources are unusual, and we believe that it is not due to possible artefacts, *e.g.* different UV coverages, images containing negative depression around the source, image misalignment at 240 and 610 MHz, etc. Also, these results do not support the known formation scenarios, discussed below, in which the wings are interpreted as relics of past radio jets and the active lobes as the newer ones.

Furthermore, the results from this class of sources is consistent with earlier results that there is no trend of spectral index with jet side at any brightness level, which has been a subject of considerable debate (Dennett-Thorpe et al. 1999, 2002; Black et al. 1992).

6.2 Formation models

The most intriguing fact about X-shaped radio galaxies is the apparently small number of sources of X-shape. Two possible explanations for the small number are, (i) they are very exotic objects that form only rarely and under extraordinary circumstances, and (ii) they are normal radio galaxies that are currently in a short-lived and/or rare phase of their evolution (Rottmann 2001). In order to explain these, it is necessary to understand the formation process responsible for the X-shaped phenomenon. We briefly introduce the key formation mechanisms and discuss them in the light of existing observational results.

6.2.1 Backflow

Leahy & Williams (1984) have argued in favour of backflow being responsible for the formation of the wings of X -shaped sources. Backflow is formed by jet material that is released by the hot spots and is then streaming back towards the host galaxy. In the model, the backflow material remains collimated until it meets the backflow from the opposite hot spot and expands laterally into a fat disk oriented perpendicular to the radio lobe axis. For physical conditions prevailing in the lobes of radio galaxies, with typical advance speed of the hotspots of a few per cent of c , high apparent backflow speeds have been inferred with roughly constant ratio of the speed of advance and the speed of backflow (Scheuer 1995). Assuming backflow velocities close to magnetosonic sound speed, though real flows occur at lower speeds, and typical secondary lobe lengths of a few hundred kiloparsec, one requires a duration of the order of a few 10^7 year for matter to flow from the core to the tips of the secondary lobes. This is less than the radiative age, $\sim 10^8$ year, of X -shaped sources assuming equipartition of energy between the radiating particles and magnetic field and 610 MHz as the break frequency of the injected electron population, and/or the typical radio source lifetime of 10^8 year (Rottmann 2001). Furthermore, this being an optimistic estimate, the true lobe lengths are larger if projection effects are taken into account, which would increase the required flow speeds. On top, once the backflowing material leaves the primary lobes and has to penetrate into the ambient medium we expect the flow to be decelerated by ram-pressure. Therefore, the required flow duration will thus be closer to a few 10^8 year, which would make backflow unlikely as the dominant formation scenario unless X -shaped sources prove to be unusually old.

6.2.2 Buoyancy

On morphological grounds, the lobes of a radio galaxy have a lower density than the surrounding medium (Williams 1991). Therefore, it is expected that buoyancy may have an impact on the large scale morphology of the radio lobes. Worrall, Birkinshaw & Cameron (1995) have applied such a buoyancy model to NGC 326 and is unable to account for the formation of X -shaped radio galaxies. X-ray studies of gaseous environment of several such sources were not able to detect significant cluster gas emission (Kraft et al. 2005) with the exception of NGC 326. Although, this might be due to lack of sensitivity, the buoyancy model is also faced with the problem of rotational symmetry of X -shaped radio galaxies. The two angles between the primary and secondary lobes of an X -shaped source are typically equal to within $\pm 10^\circ$, and if buoyancy would be a dominant formation process one would expect to find a more random distribution of these angles (Rottmann 2001). Also, the radio source must do significant work on the medium, and the total work must be comparable to the stored energy within the lobes (Kaiser & Alexander 1997, 1999). Typically, the time-scale for formation of such sources, or the corresponding radius out to which the source expanded, is the age of the source times the average Mach number (< 1) for expansion (Alexander 2002), which is an order of magnitude less than age of the source. In addition, the swept-up gas would become Rayleigh-Taylor unstable since the density of the co-

coon is very much less than the external swept-up material (Scheuer 1974).

Therefore, we also conclude that buoyancy will influence the large scale structure of radio galaxies only in dense cluster environments, as is seen for wide-angle-tail radio sources in cluster of galaxies, and it is implausible that buoyancy, without a favourable configuration of the interstellar medium or intergalactic medium, would influence the structure of X -shaped sources.

6.2.3 Conical precession

The conical precession model (Parma, Ekers & Fanti 1985; Mack et al. 1994) requires not only a fortuitous angle between the precession cone and angle to the line of sight, but also a happy accident of the positions at which the source first switched on and its position now. It therefore seems unlikely that we can explain the number of such sources seen, or the lack of other related sources (Leahy & Parma 1992).

More importantly, the morphologies of these sources do not seem to fit conical precession model (Dennett-Thorpe et al. 2002). Structures linking the wing and the lobe should at least be detected at low radio frequencies, if the morphology arose from a special projection of a slowly precessing source. Instead, in almost all the sources, there is a notable lack of such a feature. Furthermore, the wings being embedded well into the base also argues against any interpretation in terms of slow motion of the jet axis. Given these arguments, it is unimaginable that such precession can be used as an explanation for X -shaped sources.

6.2.4 Reorientation of the jet axis

Although, at this point, we conclude that the most likely formation process of X -shaped radio galaxies is reorientation of their jet axis due to a minor merger, an apparent contradiction of the model is posed by the small number of X -shaped radio galaxies as compared to the rather large number of minor merger events. The typical duration of the AGN phase is $\sim 10^7$ yr. Since, time scale for jet reorientation is short, $\lesssim 10^7$ yr (Dennett-Thorpe et al. 2002), or it occurs instantaneously (Merritt & Ekers 2002), Merritt & Ekers (2002) predict both types of source, X -shaped galaxy and radio galaxy, to be visible for a similar time. In other words, similar number of sources for both types are expected.

Certainly, selection effects due to projection and beaming can conceal the X -shaped nature of some sources on unfavourable viewing angles. For moderate intrinsic angles the fraction of sources hidden by selection effects is $\sim 25\%$ (Rottmann 2001). This suggests that, unless there is a large, hidden population of objects with very small reorientation angles, selection effects are not significant and insufficient to account for small number of X -shaped sources. Another problem for the connection of merging and reorientation arises when inspecting the environments in which the hosts of X -shaped sources are embedded. None of the known sources lay in dense clusters, only a few sources seem to be located in small, poor clusters or groups and rest of the sources seem to be isolated field galaxies. Although, the latter problem, could be reconciled in a minor merger model,

leading to a sudden flip in the direction of any associated jet (Merritt 2004), we still need to address the small number of X-shaped radio galaxies as compared to the rather large number of minor merger events.

6.3 Implications on the formation models

We now discuss the implications on the assumptions of the spectral ageing method and discuss what could be the realistic formation model of X-shaped sources.

6.3.1 The assumptions of the spectral ageing method

It is possible that the assumptions used in the spectral ageing method for estimating the age needs to be investigated. Due to the presence of all category of sources, A, B & C, one of the assumptions, the low-surface-brightness wings are in the process of becoming new active jets, mentioned earlier (Lal & Rao 2005) does not seem true. Furthermore, presence of exotic reacceleration mechanism is unlikely because of absence of any shock signatures. Also, the high degree of polarised emission observed in the wings (Rottmann 2001) indicates that the stochastic reacceleration by plasma turbulence is not applicable in the wings of these sources. A combination of rest of the two assumptions, *i.e.* the injection spectral index is varying (Palma et al. 2000), and presence of a gradient in magnetic field across the source, together with curved electron energy spectrum (Blundell & Rawlings 2000) could explain each of these X-shaped sources individually, but a single model presently seems implausible.

6.3.2 Environments of X-shaped sources

It has also been argued that the X-shaped morphology is essentially a hydrodynamic phenomenon which is a result of supersonic or buoyant flow of radio plasma in an asymmetric gas distribution. Leahy & Williams (1984) and Worrall, Birkinshaw & Cameron (1995) argues that the X-shaped radio morphology is a result of strong backflow of material behind the terminal hot spots of radio galaxy jets and subsequent buoyant evolution of the wings. In this model, the lobes and the wings must have been supersonic at some time in the past, but are now evolving buoyantly. Capetti et al. (2002) hypothesized that the X-shaped morphology is a direct result of the supersonic expansion and/or inflation of the lobe into an elliptical atmosphere and that all radio galaxies in such environments should exhibit this phenomenon. In this scenario, both the lobes and the wings should be enormously overpressurized relative to the ambient medium (Kraft et al. 2005). Although inhomogeneous and incomplete, the sample of X-shaped sources show diverse spectral morphologies and a single model with similar dynamics of the backflow/buoyancy, jet velocities, density contrast between the jet and the ambient medium, temperature and density profile of the medium, and morphology of ambient medium for these sources would be a challenge.

6.3.3 Existing formation models versus Merger of two AGNs

Lal & Rao (2005) proposed to use the low frequency spectra at different locations in the source, to distinguish between the formation models for these sources. In the simplest picture, the low-surface-brightness wings would have an older population of the electrons and therefore should have steeper spectral index as compared to the active high-surface-brightness radio lobes. But, the two categories of sources, namely, sources showing the wings to be of flatter spectral indices as compared to the active lobes (category A) and sources showing the wings and the active lobes to be of comparable spectral indices (category B), listed above does not support this simple picture. Instead, the third category of sources, five of the twelve sources, supports this picture. Furthermore, none of the models mentioned earlier, support the radio results from the first two categories of sources. On top, each of these models have their own limitations, which are independent of our spectral results.

Begelman, Blandford & Rees (1980) first suggested the possibility that AGN might contain massive binary black hole. The proposition is justified via., (i) the nuclei of most galaxies contain massive black hole and (ii) galaxies often merge. More importantly, all radio images of the sample of X-shaped sources show the wings and the lobes to be embedded well into the base and argues in favour of unresolved, coalescing binary AGN system. In order to understand, if the X-shaped sources are indeed examples of unresolved binary AGN systems, with two pairs of jets associated with two unresolved AGNs, several methods have been suggested, *e.g.* an indirect hint for the presence of binary AGNs is using *HST* to identify inwardly decreasing surface brightness profiles in the galaxy. We have re-analyzed the archived snapshot *HST* data for 3C 52, 3C 136.1, 3C 223.1, 3C 315, 3C 403 and 3C 433. A close inspection of the deconvolved brightness profiles in each source does not suggest a centrally depressed, nearly flat core. But is this due to obscuration of the core by the dusty disk (de Koff 1996), needs to be followed with new deep images.

6.4 Do X-shaped sources form a single class?

Based on the GMRT results presented above, we conclude that earlier models do not explain the formation scenario for the X-shaped sources. Only viable model is the ‘alternative’ model, *i.e.* the X-shaped sources consists of two pairs of jets, which are associated with two unresolved AGNs (Lal & Rao 2005). This ‘alternative’ model not only explains earlier observational results, it also explains our low frequency spectral results. The proposition also supports the small number of X-shaped sources, as the frequency of merger of two field AGNs is small and is definitely smaller than the number of minor merger events. Hence, we believe that every X-shaped source consist of an unresolved binary AGN, giving two pairs of jets corresponding to two AGNs. Whether or not the central binary black hole can actually account for the formation of X-shaped radio galaxies mainly depends on the timescales of shrinking of separation radii and final merging of the binary system. In other words, it critically depends on the evolution and the stability of the binary system (Begelman, Blandford & Rees 1980).

We suggest high resolution, multi-frequency, phase-referenced very-long-baseline-interferometry (VLBI) imaging of *X*-shaped sources, in order to determine the recent active jet and investigate if these sources are example of resolved binary AGN systems (Sudou, Iguchi & Murata 2003; Rodriguez et al. 2006). In addition, we also suggest deep *HST*, *Chandra* images to detect binary supermassive black holes, and a search process using the images from the VLA NVSS (Condon et al. 1998) and FIRST (Becker, White & Helfand 1995) surveys with a goal of increasing the total number of *X*-shaped radio sources, thereby forming a homogeneous complete sample. Additional observational results and wisdom gained from it would allow us to understand these sources in a statistical manner.

7 CONCLUSIONS

We have presented the lowest frequency images of the sample of *X*-shaped sources at 240 and 610 MHz, and our radio spectral results have been instrumental in testing the formation scenario of these sources. The measurements presented here represent most of the database that we require for rigorously testing and understanding the formation models of these sources. Based on our careful analysis and estimation of the possible systematic errors, along with the integrated radio flux densities and the spectral indices from it at several locations across each of these sources, we show that these sources divide into following three categories:

(A) Sources in which the wings are of flatter spectral indices than the active lobes, namely, 4C 12.03, 3C 223.1 and B1059+169.

(B) Sources in which the wings and the active lobes have comparable spectral indices, namely, 3C 192, B2 0828+32, 4C 48.29 and 3C 403.

(C) Sources in which the wings are of steeper spectral indices than the active lobes, namely, NGC 326, 3C 52, 3C 136.1, 3C 315 and 3C 433.

These GMRT results do not support earlier known formation models for the *X*-shaped sources. While it is equally probable that the three categories, A, B & C, of sources are unrelated to one another, a single model to explain these sources is a challenge. Currently, only possible model is our ‘alternative’ model, *i.e.* the *X*-shaped sources consists of two pairs of jets, which are associated with two unresolved AGNs (Lal & Rao 2005).

There is definitely a need to understand the proposed formation scenario for *X*-shaped sources and hence, follow-up work is necessary. Future, VLBI results, together with deep *HST*, *Chandra* images and results from a larger homogeneous complete sample of *X*-shape sources would be useful in constraining any possible formation model.

ACKNOWLEDGMENTS

We thank the staff of the GMRT who have made these observations possible. GMRT is run by the National Centre for Radio Astrophysics of the Tata Institute of Fundamental Research. We also thank the anonymous referee for his/her prompt review of the manuscript and for comments that lead

to improvement of the paper. DVL thanks R Nityananda and M Hardcastle for discussions and several useful comments. This research has made use of the NASA/IPAC Extragalactic Database, which is operated by the Jet Propulsion Laboratory, Caltech, under contract with the NASA, and NASA’s Astrophysics Data System.

REFERENCES

- Alexander, P., 2002, MNRAS, 335, 610
 Alexander, P., Leahy, J.P., 1987, MNRAS, 225, 1
 Baars, J.W.M., Genzel, R., Pauliny-Toth, I.I.K., Witzel, A., 1977, A&A, 61, 99
 Becker, R.H., White, R.L., Edwards, A.L., 1991, ApJS, 75, 1
 Becker, R.H., White, R.L., Helfand, D.J., 1995, ApJ, 450, 559
 Begelman, M.C., Blandford, R.D., Rees, M.J., 1980, Nature, 287, 307
 Blundell, K.M., Rawlings, S., 2000, AJ, 119, 1111
 Black, A.R.S., Baum, S.A., Leahy, J.P., Perley, R.A., Riley, J.M., Scheuer, P.A.G., 1992, MNRAS, 256, 186
 van Breugel, W., Helfand, D., Balick, B., Heckman, T., Miley, G., 1983, AJ, 88, 40
 van Breugel, W., Jägers, W., 1982, A&AS, 49, 529
 Burns, J.O., Gregory, S.A., Holman, G.D., 1981, ApJ, 250, 450
 Capetti, A., Zamfir, S., Rossi, P., Bodo, G., Zanni, C., Masaglia, S., 2002, A&A, 394, 39
 Condon, J.J., Cotton, W.D., Greisen, E.W., Yin, Q.F., Perley, R.A., Taylor, G.B., Broderick, J.J., 1998, AJ, 115, 1693
 Dennett-Thorpe, J., Bridle, A.H., Laing, R.A., Scheuer, P.A.G., 1999, MNRAS, 304, 271
 Dennett-Thorpe, J., Scheuer, P.A.G., Laing, R.A., Bridle, A.H., Pooley, G.G., Reich, W., 2002, MNRAS, 330, 609
 Ekers, R.D., Fanti, R., Lari, C., Parma, P., 1978, Nature, 276, 588
 Fanaroff, B.L., Riley J.M., 1974, MNRAS, 167, 31P
 Feretti, L., Giovannini, G., Gregorini, L., Parma, P., 1983, A&A, 126, 311
 Ficarra, A., Grueff, G., Tomassetti, G., 1985, A&AS, 59, 255
 Gregory, P.C., Condon, J.J., 1991, ApJS, 75, 1011
 Gopal-Krishna, Biermann, P.L., Wiita, P.J., 2003, ApJL, 594, 103
 Gower, J.F.R., Scott, P.F., & Wills, D. 1967, Mem.RAS, 71, 49
 Hardcastle, M.J., Alexander, P., Pooley, G.G., Riley, J.M., 1997, MNRAS, 288, 859
 Heckman, T.M., O’Dea, C.,P., Baum, S.A., Laurikainen, E., 1994, ApJ, 428, 65
 Högbom, J.A., 1979, A&AS, 36, 173
 Kaiser, C.R., Alexander, P., 1997, MNRAS, 286, 215
 Kaiser, C.R., Alexander, P., 1999, MNRAS, 305, 707
 Kellermann K.I., Pauliny-Toth, I.I.K., Williams, P.J.S, 1969, ApJ, 157, 1
 de Koff, S., Baum, S.A., Sparks, W.B., Biretta, J., Golombek, D., Macchetto, F., McCarthy, P., Miley, G.K., 1996, ApJS, 107, 621

- Kraft, R.P., Hardcastle, M.J., Worrall, D.M., Murray, S.S., 2005, *ApJ*, 622, 149
- Kuhr, H., Witzel, A., Pauliny-Toth, I.I.K., Nauber, U. 1981, *A&AS*, 45, 367
- Laing, R.A., Riley, J.M., Longair, M.S., 1983, *MNRAS*, 204, 151
- Lal, D.V., Rao, A.P., 2005, *MNRAS*, 356, 232
- Large, M.I., Mills, B.Y., Little, A.G., Crawford, D.F., Sutton, J.M., 1981, *MNRAS*, 194, 693
- Leahy, J.P., Black, A.R.S., Denett-Thorpe, J., Hardcastle, M.J., Komissarov, S., Perley, R.A., Riley, J.M., Scheuer, P.A.G., 1997, *MNRAS*, 291, 20
- Leahy, J.P., Parma, P., 1992 in Roland, J., Sol, H., Pelletier, G., eds, *Extragalactic Radio Sources. From Beams to Jets*, Cambridge University Press, p. 307
- Leahy, J.P., Williams, A.G., 1984, *MNRAS*, 210, 929
- Mack, K.-H., Gregorini, L., Parma, P., Klein, U., 1994, *A&AS*, 103, 157
- Martel, A.R., Baum, S.A., Sparks, W.B., Wyckoff, E., Biretta, J.A., Golombek, D., Macchetto, F.D., de Koff, S., McCarthy, P.J., Miley, G.K., 1999, *ApJS*, 122, 25
- McCraithy, P., Spinard, H., van Breugel, W., 1995, *ApJS*, 99, 27
- Merritt, D., 2004, in *Coevolution of black holes and Galaxies*, Ho., L.C., Ed. (Cambridge Univ Press)
- Merritt, D., Ekers, R.D., 2002, *Sci*, 297, 1310
- Murgia, M., Parma, P., de Ruiter, H.R., Bondi, M., Ekers, R.D., Fanti, R., Fomalont, E.B., 2001, *A&A*, 380, 102
- Owen, F.N., Ledlow, M.J., 1997, *ApJS*, 108, 41
- Palma, C., Bauer, F.E., Cotton, W.D., Bridle, A.H., Majewski, S.R., Sarazin, C.L., 2000, *AJ*, 119, 2068
- Parma, P., Ekers, R.D., Fanti, R., 1985, *A&AS*, 59, 511
- Pilkington, J.D.H., Scott, P.F., & Wills, D. 1965, *Mem.RAS*, 69, 183
- Rees, M.J., 1978, *Nat*, 275, 516
- Rottmann, H., 2001, PhD thesis, Rheinischen Friedrich-Wilhelms-Universität Bonn
- Rodriguez, C., Taylor, G.B., Zavala, R.T., Peck, A.B., Pollock, L.K., Romani, R.W. 2006, *ApJ*, 646, 49
- Ryle, M., 1960, *J. Instn elect. Engrs*, 6, 14
- Sandage, A., 1972, *ApJ*, 178, 25
- Scheuer, P.A.G., 1974, *Sci*, 300, 1263
- Scheuer, P.A.G., 1995, *MNRAS*, 277, 331
- Steer, D., Dewdney, P., Ito, M., 2003, *Sci*, 300, 1263
- Sudou, H., Iguchi, S., Murata, Y., 2003, *Sci*, 300, 1263
- Swarup, G., Ananthakrishnan, S., Kapahi, V.K., Rao, A.P., Subrahmanya, C.R., Kulkarni, V.K., 1991, *Cu. Sc.*, 60, 95
- 2003, *ApJ* 126, 113
- Ulrich, Marie-Helene, Rönnback, Jari, 1996, *A&A*, 313, 750
- Wirth, A., Smarr, L., Gallagher, J.S., 1982, *AJ*, 87, 602
- White, R.L., Becker, R.H., 1992, *ApJS*, 79, 331
- Worrall, D.M., Birkinshaw, M., Cameron, R.A., 1995, *ApJ*, 449, 93
- Zirbel, E.L., 1997, *ApJ*, 476, 489
- Zwicky, F., Kowal, C.T., 1968, *Catalogue of Galaxies and Clusters of galaxies*, Pasadena, Caltech